POLITECNICO
MILANO 1863

SCUOLA DI INGEGNERIA INDUSTRIALE
E DELL'INFORMAZIONE

Preliminary design and FEM analysis of a 3D printed prosthetic foot.

TESI DI LAUREA MAGISTRALE IN
MECHANICAL ENGINEERING
INGEGNERIA MECCANICA

Author: **Aswinraj Elumalai**

Student ID:	10870626
Advisor:	Prof. Andrea Bernasconi
Academic Year:	2024-25

Abstract:

Additive manufacturing is transforming the prosthetic field by enabling the creation of customized, patient-specific devices with intricate geometries that traditional manufacturing methods often cannot achieve. This technology allows for rapid prototyping, reducing development time and costs, while offering flexibility to tailor prosthetics to the unique anatomical requirements of each user. Additive manufacturing techniques facilitate the production of lightweight yet robust structures, improving overall comfort and performance. Moreover, the ability to integrate multiple materials within a single build enhances the functionality and durability of prosthetic devices. In this thesis, preliminary 3D printed prosthetic foot design has been studied, to understand if 3D printing technology can be considered a good manufacturing process to create such kind of device. The study begins with a 2D analysis to evaluate the structural behaviour of a prosthetic foot composed entirely of TPU material, comparing it with a TPU foot incorporating a rigid ABS keel. A key observation from this 2D analysis is that the inclusion of an ABS keel significantly enhances the stiffness of the foot, thereby reducing its maximum deflection under loading conditions. The prosthetic foot consists of five main components: the inner foot, external cover, keel, pyramid connector, and screws. The keel and inner foot geometries were determined through a traditional iterative approach. Subsequently, a 3D analysis was performed under three distinct loading conditions—toe-off, mid-stance, and heel-strike—in accordance with ISO 10328: 2016 standards at the P5 loading level. The key finding in this study is the impact of ABS keel on the stiffness of foot, which is made up of TPU, a highly flexible material. The prosthetic foot successfully endured the applied static load conditions, with the stress generated in each component remaining within the ultimate tensile strength of the materials across all cases, and the maximum deflection underload falling within acceptable limits. Furthermore, a fatigue assessment of the prosthetic foot design revealed that it failed to meet the required number of fatigue cycles before failure.

Key-words: Finite element analysis, Prosthetic foot, Additive manufacturing, Thermoplastic polyurethane (TPU), Acrylonitrile Butadiene Styrene (ABS)

Abstract in lingua Italiana:

La manifattura additiva sta trasformando il campo delle protesi, consentendo la creazione di dispositivi personalizzati e specifici per il paziente con geometrie complesse che i metodi di produzione tradizionali spesso non riescono a raggiungere. Questa tecnologia permette la prototipazione rapida, riducendo i tempi e i costi di sviluppo, offrendo al contempo la flessibilità di adattare le protesi ai requisiti anatomici unici di ciascun utente. Le tecniche di manifattura additiva facilitano la produzione di strutture leggere ma robuste, migliorando il comfort e le prestazioni complessive. Inoltre, la possibilità di integrare più materiali in una singola costruzione migliora la funzionalità e la durata dei dispositivi protesici. In questa tesi, è stato studiato un design preliminare di una protesi del piede stampato in 3D, per capire se la tecnologia di stampa 3D può essere considerata un buon processo di fabbricazione per creare tale dispositivo. Lo studio inizia con un'analisi 2D per valutare il comportamento strutturale di una protesi del piede composta interamente da materiale TPU, confrontandola con una protesi in TPU che incorpora una chiglia rigida in ABS. Una osservazione chiave di questa analisi 2D è che l'inclusione di una chiglia in ABS aumenta significativamente la rigidità del piede, riducendo così la sua deflessione massima sotto carico. La protesi del piede è composta da cinque componenti principali: il piede interno, la copertura esterna, la chiglia, il connettore a piramide e le viti. Le geometrie della chiglia e del piede interno sono state determinate tramite un approccio iterativo tradizionale. Successivamente, è stata eseguita un'analisi 3D sotto tre diverse condizioni di carico: toe-off, mid-stance e heel-strike, in conformità con gli standard ISO 10328: 2016 al livello di carico P5. Il principale risultato di questo studio è l'impatto della chiglia in ABS sulla rigidità del piede, composto da TPU, un materiale altamente flessibile. La protesi del piede ha resistito con successo alle condizioni di carico statico applicato, con le sollecitazioni generate in ogni componente che rimangono entro i limiti di resistenza a trazione ultima dei materiali in tutti i casi, e la deflessione massima sotto carico che rientra nei limiti accettabili. Inoltre, una valutazione della fatica del design della protesi del piede ha rivelato che non soddisfa il numero di cicli di fatica richiesti prima del fallimento.

Parole chiave: Analisi degli elementi finiti, Piede protesico, Produzione additiva, Poliuretano termoplastico (TPU), Acrilonitrile Butadiene Stirene (ABS)

Contents

Abstract: ii
Abstract in lingua Italiana: iii
Acknowledgement vi
Introduction 1
1. State of the art 3
1.1 Prosthetic Device 3
1.1.1 The purpose of a prosthesis 3
1.1.2 History of prosthetics 3
1.1.3 How war and the U.S. military inspired prosthetic advances 4
1.1.4 Foot anatomy 5
1.1.5 Prosthesis components 6
1.1.6 Gait cycle 9
1.2 Additive manufacturing (AM) Technology 10
1.2.1 Material Extrusion (MEX) 12
1.2.2 Material Extrusion with Filaments 13
1.3 Literature review 13
2. Material and Process selection: 17
2.1 Test Procedure: 19
2.2 Finite Element Analysis of Prosthetic foot: 19
2.2.1 Simplified 2D analysis: 19
2.2.2 Convergence analysis: 21
3. 2D Analysis Results: 24
4. 3D Analysis of prosthetic foot: 29
5. Results of 3D analysis 45
5.1 Toe-off case 45
5.2 Mid-stance case 47
5.3 Heel-strike case 50
6. Conclusions and Future work 55
6.1 Future works: 56

Bibliography **57**
List of Figures **59**
List of Tables **62**

Acknowledgement

The thesis study is performed together with the Roadrunnerfoot Engineering s.r.l. which is the first Italian company that designs, manufactures, and sells aids for disabled people and components for prostheses. I would like to thank Dr. Daniele Bonacini from Roadrunnerfoot Engineering for providing me with the opportunity to work on this topic. Their resources and support have been crucial in the successful completion of this thesis. I am thankful for the experience and knowledge I have gained.

I would also like to extend my sincere thanks to Prof. Andrea Bernasconi, for his invaluable guidance, support, and encouragement throughout the course of my thesis work. His expertise and insights have been instrumental in shaping this thesis, and I am truly grateful for his mentorship.

Introduction

Prosthetic technology has made significant advancements, providing individuals with lower-limb amputations with the ability to regain mobility. While traditional prosthetic feet are typically designed with rigid structures, recent innovations in additive manufacturing have led to the development of lightweight and customizable alternatives. 3D printing offers several benefits in prosthetic fabrication, including reduced production time, lower costs, and decreased overall weight. Conventional prosthetic manufacturing involves complex procedures and high expenses, often requiring amputees to wait several weeks—typically between three to six—for production and delivery. In contrast, 3D-printed prosthetics are more cost-effective, have a significantly shorter production time, and utilize readily available materials, making it possible to manufacture a prosthetic within a single day.

Despite these advantages, optimizing the mechanical strength, durability, and material selection of 3D-printed prosthetic feet remains a challenge. This research aims to address these issues by designing and evaluating prosthetic foot utilizing additive manufacturing techniques. The study involves the preliminary design and structural analysis of a 3D-printed prosthetic foot, incorporating computer-aided design (CAD) and finite element analysis (FEA) to assess its performance under real-world loading conditions. By developing an affordable, lightweight, and customizable prosthetic foot, this study seeks to enhance accessibility for amputees globally. The findings will aid in refining additive manufacturing techniques for medical applications, promoting more efficient and personalized prosthetic solutions. This thesis is structured as follows:

- Chapter One: An overview of prosthetic devices and their purpose followed by foot anatomy, gait cycle and prosthesis components are reported in this chapter. Then 3D printing technology is investigated, starting from the description of Additive Manufacturing and fused filament fabrication. Some previous 3D printed lower limb prosthesis studies are also reported.

- Chapter Two: Material properties are here investigated. Starting with data sheets provided by filament suppliers. Estimating the young's modulus based on the data available in the technical data sheet. The static and fatigue testing procedure according to the ISO standard are reported. The 2D finite element model with corresponding boundary and loading conditions, and estimation of mesh size that provides accurate results with the help of convergence study are also reported in chapter two.

- Chapter Three: The results coming from 2D finite elements analysis are reported. The results are compared with the experimental values provided by the Roadrunnerfoot Engineering company. The comparison of 2D foot without and with the addition of keel is investigated in this chapter.

- Chapter Four: The final shape and size of some components of the prosthetic foot are determined in this chapter using traditional iterative design approach, followed by simulation according to ISO standard provided in chapter two using Abaqus software. The final design of prosthetic foot along with all components are proposed here.

- Chapter Five: The results obtained from 3D finite element analysis are reported here. The results are compared with the experimental values provided by the Roadrunnerfoot Engineering company and a critical discussion of the results is reported.

- Chapter Six: Conclusions are here reported, with possible suggestions for future activities to continue the 3D printed prosthetic foot study.

Chapter one

1. State of the art

1.1 Prosthetic Device

A prosthesis is an artificial device used to replace all or part of a missing limb. Prostheses are often used by someone who has experienced limb loss due to injury, accident, or illness, but they can also be used by someone with a congenital condition that results in a limb difference. Unlike knee or hip replacements ("endoprostheses"), which are implanted in the patient's limb, prostheses are worn by the user by attaching it to their residual limb. While not everyone with a limb difference or limb loss needs a prosthesis, the right device can empower users in many ways [1].

1.1.1 The purpose of a prosthesis

The basic purpose of a prosthetic device is to restore the functionality and mobility of a missing limb, making it easier to take part in daily activities, hobbies, work tasks, and more. Prostheses can also improve users' quality of life, empowering them to be as active as they want and are able to be – whether that means moving safely around their house or being a high-performance athlete. For people who have experienced limb loss, a prosthetic device can also help reduce the emotional impact of an accident or injury [1].

1.1.2 History of prosthetics

The oldest known prosthetics are two different artificial toes from ancient Egypt. One prosthetic toe, known as the "Greville Chester toe," was made from cartonnage, which is a kind of papier-mâché made from glue, linen, and plaster. It is thought to be between 2,600 and 3,400 years old, though its exact age is unknown. The other prosthetic, a wooden and leather toe known as the "Cairo toe," is estimated to be between 2,700 and 3,000 years old. It is thought to be the earliest known practical artificial limb due to its flexibility and because it was refitted for the wearer multiple times. Approximately 300 years later—300 B.C.—in Italy, an ancient Roman nobleman used a prosthetic leg known as the "Capua leg" (Figure 1). The leg was made of bronze

and hollowed-out wood and was held up with leather straps. Other known early prosthetics include artificial feet from Switzerland and Germany, crafted between the 5th and 8th centuries. These were made from wood, iron, or bronze and may have been strapped to the amputee's remaining limb [2].

Figure 1: Capua leg (replica).

1.1.3 How war and the U.S. military inspired prosthetic advances

Soldiers who lost their limbs in battle often used early artificial limbs made of wood or iron. For example, about 2,200 years ago, the Roman general Marcus Sergius Silus lost his right hand during the Second Punic War. He had it replaced with an iron one that was designed to hold his shield. Knights of the Middle Ages sometimes used wooden limbs for battle or to ride a horse. And in the 16th century, the French surgeon Ambroise Paré designed some of the first purely functional prosthetics for soldiers coming off the battlefield. He also published the earliest written reference to prosthetics.

Then came the American Civil War in 1860. The record number of amputees from the war caused the number of patents for prosthetics to almost quadruple. One of these patents was for a wooden leg called the "Hanger limb" (Figure 2). It was the first to use rubber in the ankle and cushioning in the heel, showing that inventors understood they needed to make prosthetics less painful for amputees to wear [2].

Figure 2: An Artificial leg from American civil war

1.1.4 Foot anatomy

In this thesis work, a study of the 3D printed material used for creation of a foot prosthesis has been conducted. It is important to describe the foot anatomy, and what needs to be recreated to reproduce a gait as naturally as possible.

Human feet are a brilliant example of evolutionary engineering. They allow us to walk and run upright while absorbing impact that can be many times one's body weight. By the time a person reaches 50 ages, a person would have likely put 75,000 miles on them. They are highly specialized in structure and function, in part by how many bones are in a foot: 26 bones – about a quarter of all the bones in the body [3]. They include:

- Seven tarsals at the back of the foot
- Five metatarsals in the middle of the foot
- 14 phalanges in the toes

They're connected by 33 joints and more than 100 tendons and ligaments. The simplified anatomy of human foot is shown in Figure 3.

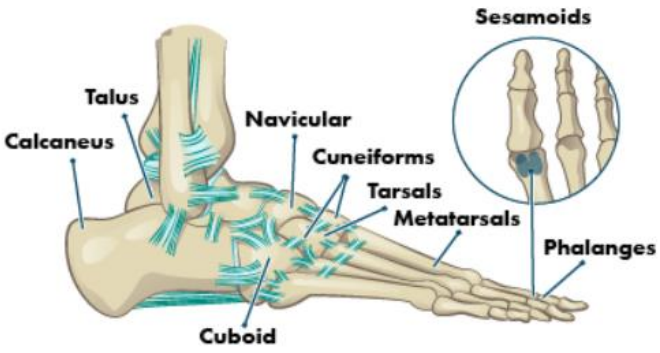

Figure 3: Anatomy of human foot.

The tarsals are a group of bones that form the ankle and the back part of the foot. They include talus, calcaneus, cuboid, cuneiforms and navicular. Metatarsals are the five long bones, just below the phalanges or toe bones. One can usually feel these bones with their fingers. Each metatarsal has three parts: a base, a middle shaft and a head that connects to the phalanges. The first metatarsal connects to the big toe and is important for forward movement. The other four metatarsals provide stability to the front of the foot. Phalanges are the 14 bones that make up the toes. The phalanges in the feet are like those in the hand, but they're shorter, stronger and less mobile. They're also shorter than the metatarsals. Like the thumb, the big toe has two phalanges. The others have three – a base, shaft and head. Sesamoids are the two small, pea-shaped bones embedded in a tendon below the first metatarsal (closest to the big toe) on the bottom of the foot. Their job is to strengthen and reduce stress on the tendon [3].

Joints are formed wherever two or more bones meet. Each foot's 33 joints have two essential roles: bearing weight and propelling the body forward when walking or running. To do this, joints must be both stable and flexible. The foot's flexibility comes from the large number of joints, many of which involve more than two bones. Over 100 tendons, ligaments and muscles hold the bones and joints in the foot together. Tendons attach muscles to bones; ligaments attach bones to other bones [3].

1.1.5 Prosthesis components

In this section different components of prosthesis will be analyzed and briefly discussed, paying particular attention to the prosthetic foot which is focus of this thesis work. It is possible to divide the whole prosthetic limb into different components, each one with its own function, to simulate the realistic behaviour of a human inferior limb. These different components are [4]:

Socket - The socket (Figure 4) connects your residual limb to your prosthetic leg and is the foundation of the prosthetic leg. A proper fit is essential to ensure that you can function comfortably and well. Since no two residual limbs are the same, the socket is custom-designed and manufactured to suit the shape of your residual limb and to accommodate individual shape and skin patterns.

Liner - The liner (Figure 4) serves as a protective barrier between your skin and the socket. Because the socket and suspension are fundamental to the effective functioning of a prosthetic leg, it is extremely important to select the right liner.

Figure 4: Liner on the inner surface of socket.

Prosthetic knee - Depending on the location of the amputation, prosthetic leg may or may not feature a knee. A prosthetic knee (Figure 5) mimics the function of a biological knee by providing safety, symmetry and smooth movement when walking. It also provides stability when standing and a range of motion that makes sitting and kneeling possible. The knee is one of the most complicated joints in the human body, so designing a prosthesis that functions like a biological knee can be challenging. If the design forces the user to walk in an unnatural way, they may experience back and hip pain. Or if the knee doesn't suit the user's physical requirements, it may cause them to fall. Prosthetic knees can be divided into mechanical or bionic (computerized) knees.

Figure 5: Hydraulic knee joint, produced by Roadrunnerfoot Engineering.

Prosthetic foot - A prosthetic foot imitates the function of a biological foot by providing a safe platform, handling differences in terrain and allowing the individual to walk in a natural, symmetrical way. The foot is the main prosthetic component responsible for absorbing the shock generated by impact on the ground. Prosthetic feet are available in a wide range to reflect your lifestyle and individual requirements [4].

Prosthetic feet can be made from wood, rubber, urethane, titanium, fiber glass and carbon fiber. They can be lightweight, energy-storing, or dynamic and some can allow adjustability of heel height. All prosthetic feet should provide passive plantar flexion in early stance, neutral position in mid stance and toe hyperextension in late

stance. Among different designs of feet, it is worth mentioning those most common in use.

Non-Articulated Feet – also known as SACH (Solid Angle Cushion Heel) consist of a rigid foot without ankle articulation, where the heel absorbs the shock, and the forefoot simulates the dorsal flexion of the foot. An example of such SACH foot is shown in Figure 6. There are feet with different degrees of heel amortization offered in the market. Despite having a very simple design, SACH feet respond to functional necessities in all the phases of the gait. The SACH foot is primarily suited for low-activity users due to its durability, low cost, and waterproof nature [5].

Figure 6: An example of prosthetic SACH foot, produced by Ottobock

Articulated Feet - Articulated prosthetic feet (Figure 7), available in single-axis and multi-axis designs, aiming to replicate the natural movements of the anatomical foot more effectively. Single-axis feet facilitate plantarflexion and dorsiflexion, improving knee stability, especially for transfemoral (TF) amputees. Conversely, multi-axis feet offer inversion and eversion, adapting better to uneven terrain and reducing stress on the residual limb. These feet provide greater mobility and comfort compared to SACH feet but come with drawbacks, including heavier weight, higher cost, and increased maintenance requirements [5].

Figure 7: An example of prosthetic articulated feet, produced by Ottobock

Dynamic response or energy return feet - utilize carbon fiber keels (Figure 8) that function as springs, storing and releasing energy during gait. This feature provides a "push-off" effect, leading to more natural and efficient movement. These feet are particularly beneficial for moderate to high-activity users, as they support varying walking speeds, quick directional changes, and longer distances [5].

Figure 8: An example of prosthetic articulated feet, produced by Ottobock

Finally, cosmetics are used, it is the exterior shape of the foot and has the function to reproduce the appearance of a natural human foot. Usually, it is composed of plastic pink material or some spongy material with a color close to the one of the human skins.

1.1.6 Gait cycle

Initiating gait requires a stable upright body position. Functioning postural reflexes is necessary to assume and sustain a stable position. To start walking, one leg is raised and directed forward by flexing the hips and knee. Activation of the supporting contralateral leg and trunk muscles moves the body's center of gravity over the weight-bearing leg and forward. The heel of the swinging leg is then placed on the ground. The body weight is gradually shifted to the sole and then onwards to the toes. During mid-stance, the opposite leg is lifted and moves forward until the heel strikes the ground. Meanwhile, the body is held upright, the shoulders and pelvis remain relatively level and each arm swings in the direction opposite to that of its ipsilateral leg. The gait cycle (Figure 9) is divided into the stance and swing phase. The stance phase constitutes approximately 60 % of the gait cycle and is subdivided into initial contact (heel strike), loading response, mid-stance, terminal stance and pre-swing. Both feet are on the ground at the beginning and end of the stance phase. Each of these two double support periods lasts for approximately 10–12 % of the gait cycle. The swing phase takes up about 40 % of the gait cycle and is subdivided into initial swing (toe-off), mid-swing (tibia vertical) and terminal swing, terminated by the heel striking the ground [6].

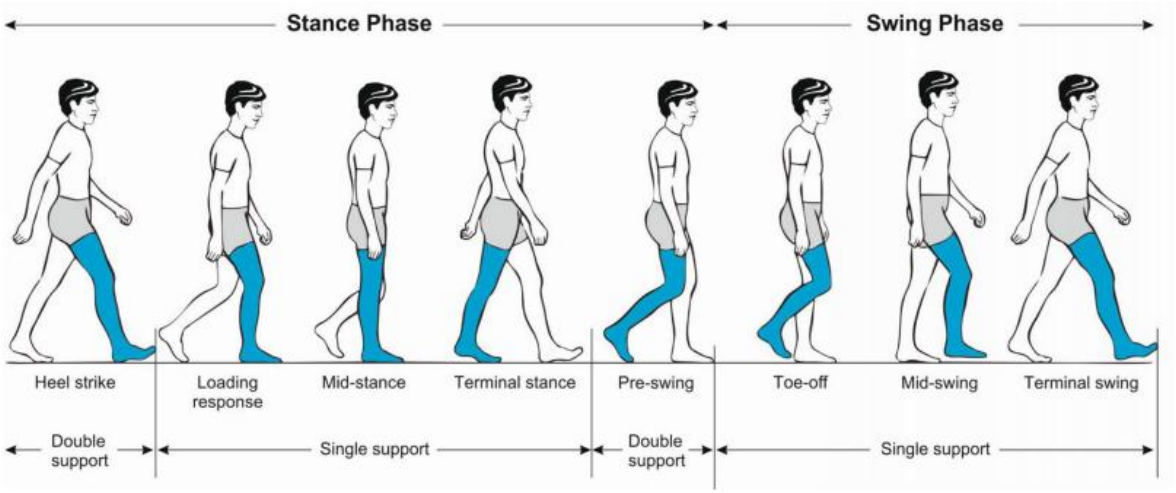

Figure 9: Phases of the normal gait cycle.

1.2 Additive manufacturing (AM) Technology

Additive manufacturing, often referred to as 3D printing, is a computer-controlled process for creating 3D objects. As the name implies, objects are built up by 'adding' material — usually plastic, ceramic, or metal powder — to a build platform in thin layers, which are hardened using a curing agent, heat, or a laser beam. The additive manufacturing process is much more complex and can be broken down into four main steps [7]:

1. Using CAD Software to Design a Model: Computer-Aided Design (CAD) plays a critical role in additive manufacturing. It's used to design and test 3D models that are viable for real-world applications.
2. Pre-Processing: covers a range of steps that must be completed between design and manufacturing. It covers two primary activities:
   2.1. Simulation Modelling: Simulation modelling is used to digitally test 3D designs before they are manufactured. These tests are used to determine the real-world structural integrity of an object i.e., whether it is likely to fail, how it might fail, and what forces it can withstand without failing
   2.2. Preparing Files for 3D printing: Once a 3D design has been tested and signed off, it's ready to be prepared for printing. To do this, a hurdle must be overcome: interoperability. Interoperability is the ability of different computer systems to exchange and make use of information. In the additive manufacturing process, the problem is simple — manufacturing machines like 3D printers don't 'understand' CAD files well enough to enable the manufacturing process. To overcome this, a file must be converted into a set of instructions that can be understood by additive manufacturing hardware. These instructions are created using 'slicer' software which converts the 3D design into 2D layers or slices which can then be used to calculate the tool path or G-Code needed to manufacture the object.

2.3. Printing:
2.4. Post-Processing: Post-processing is often the most expensive and time-consuming aspect of additive manufacturing.

Selecting the most suitable 3D printing process for the purpose is a crucial passage and can be difficult. The range of 3D printing methods and materials means that several processes are suitable for different purposes. Each process can exhibit different characteristics like dimensional accuracy, surface finish and mechanical properties, and sometimes post processing is required.

It is possible to summarize the 3D printing technologies in 7 different processes [8],

1. **Vat Photopolymerization -** A vat of liquid photopolymer resin is cured through selective exposure to light (via a laser or projector) which then initiates polymerization and converts the exposed areas to a solid part.
2. **Powder Bed Fusion -** Powdered material is selectively consolidated by melting it together using a heat source such as a laser or electron beam. The powder surrounding the consolidated part acts as support material for overhanging features.
3. **Binder Jetting -** Liquid binders (organic or inorganic) are selectively printed onto thin layers of powdered material to build up parts layer-by-layer. Some parts may be used in their as-printed "green" state; however, most metal or ceramic parts require furnace sintering to achieve full strength.
4. **Sheet Lamination -** Sheets of material are stacked and laminated together to form an object. The lamination method can use adhesives/chemistry (paper/ plastics), ultrasonic welding, or brazing (metals). Unneeded regions are cut out layer by layer and removed after the object is built.
5. **Material Jetting -** Droplets of material are deposited layer-by-layer to make parts. Common varieties include jetting a photocurable resin and curing it with UV light, as well as jetting thermally molten materials that then solidify in ambient temperatures.
6. **Material Extrusion -** Material is extruded through a nozzle or orifice in tracks or beads, which are then combined into multi-layer models. The most used technology in material extrusion is Fused Filament Fabrication (FFF).
7. **Directed Energy Deposition -** Powder or wire is fed into a melt pool which has been generated on the surface of the part where it adheres to the underlying part or layers by using an energy source such as an arc, laser, or electron beam. This is essentially a form of automated build-up welding.

This thesis will focus on Fused Filament Fabrication, which is one of the type of material extrusion additive manufacturing processes, along with thermoplastic polymer filaments (TPU and ABS)

1.2.1 Material Extrusion (MEX)

Material extrusion (MEX) consists of pushing soft material through an orifice and depositing such material in layers to build a 3D structure. Extrusion based additive manufacturing processes are among the most widely used AM processes, particularly when working with thermoplastic and thermoplastic composites. However not only thermoplastic materials can be extruded; some examples include low melting temperature metals, glass, ceramic slurries, suspensions containing graphene and other nanoparticles, silicones and concrete. Compared to other AM processes, the equipment used for MEX can be inexpensive and very easy to operate. Therefore, the main advantage of MEX is rapid economical reproduction of standard components or prototypes with a variety of polymeric materials, low melting temperature metallic alloys and other materials [9].

Most of the MEX machines are equipped with a single extrusion head, but there is the possibility of adding two or more extrusion units to allow for multi-material fabrication. The basic principle of material extrusion additive technology involves loading and liquefaction of the material, moving the material through a nozzle or orifice by applying force or pressure, plotting liquefied material according to a pre-defined path in a controlled manner, and layer-by-layer bonding of the material to itself or secondary build material to form a coherent solid structure. After a layer is completed, the build platform moves down or the extrusion head moves up, and a new layer of material is deposited and adhered onto the previous layer. Whenever necessary, support structures are included in the process to enable fabrication of complex geometrical features. Depending on the type of extruder used, one can classify Material extrusion into different types (Figure 10) [9], namely:

1. Material Extrusion with Plungers
2. Material Extrusion with Filaments
3. Material Extrusion with Screws

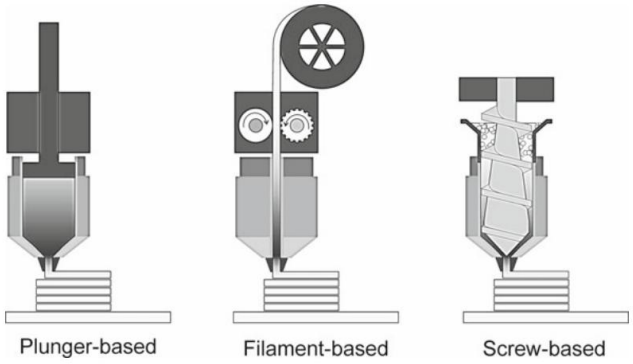

Figure 10: Material extrusion additive manufacturing types.

1.2.2 Material Extrusion with Filaments

Material extrusion of filaments was first patented by the company Stratasys and commercialized as Fused Deposition Modelling or FDM. Also, FDM is a registered trademark of the company that first introduced the technology. Therefore, an alternative terminology was introduced as Fused Filament Fabrication or FFF. FFF is the most widely used MEX technique.

The main reasons for its popularity are its safe and simple fabrication process, the low cost of the equipment and the availability of a variety of filaments for printing. In the FFF process, the filament is extruded through a nozzle and deposited on a building platform one layer at a time where it solidifies [9]. The printing chamber and bed are kept at temperatures below the material´s melting point, but higher than room temperature to promote adhesion to the printed bed and to reduce thermally induced stresses.

In conventional FFF machines, the filament is first pulled by the driving wheels and then it is pushed by the same wheels into a liquefier and later into a nozzle. Therefore, sufficient mechanical strength is required for the filament to retain its shape after being forced through the drive wheels. The filament must transfer the force provided by the driving wheels forward into the liquefier. The force that is generated by the motors must be transferred to the filament via the wheels. This transfer of force can be altered by several factors. First, the motors must generate sufficient torque. Next, the wheels must have enough friction with the filament to transfer the force from the wheels to the filament. At the same time, the filament must be strong enough to avoid shearing due to the pinching from the wheels. Finally, the filament must not buckle between the drive wheels and the entrance to the liquefier.

The main disadvantages of using MEX include a rougher surface, which is limited by the nozzle radius; the accuracy and speed can be low compared to other AM technologies; there is anisotropy of the mechanical properties, with weaker properties in the Z-direction due to the lower cohesion of the deposited layers; and support structures are needed, since the building material is deposited only where it is needed [9].

1.3 Literature review

Some previous studies on the possibility to design and then realize a 3D printed inferior limb prosthesis were conducted. As previously mentioned, the criteria that guides the engineers and designers through the realization using a 3D printer were the low cost, easier geometry and mechanical properties able to reproduce the conventional manufactured prosthetic feet.

In the paper published on 2025 [25] an iterative design framework was implemented to develop continuous fiber-reinforced additively manufactured foot

prostheses (Figure 11). The designs were assessed based on criteria defined in the American Orthotic & Prosthetic Association (AOPA) prosthetic foot project for validating dynamic-response prosthetic feet. The final design successfully satisfied the design criteria for dynamic-response prostheses, allowing a stiffness of 74 and 43 N/mm, and a percentage energy return of 88 % and 79 % under the heel and forefoot loading conditions, respectively. This study demonstrated the possibility of developing 3D-printed prosthetic feet with qualified energy storage and return performance. This published paper focuses on Energy Storage and Return (ESAR) feet, produced by Continuous Fiber-Reinforced Additively Manufacturing (CFRAM) method.

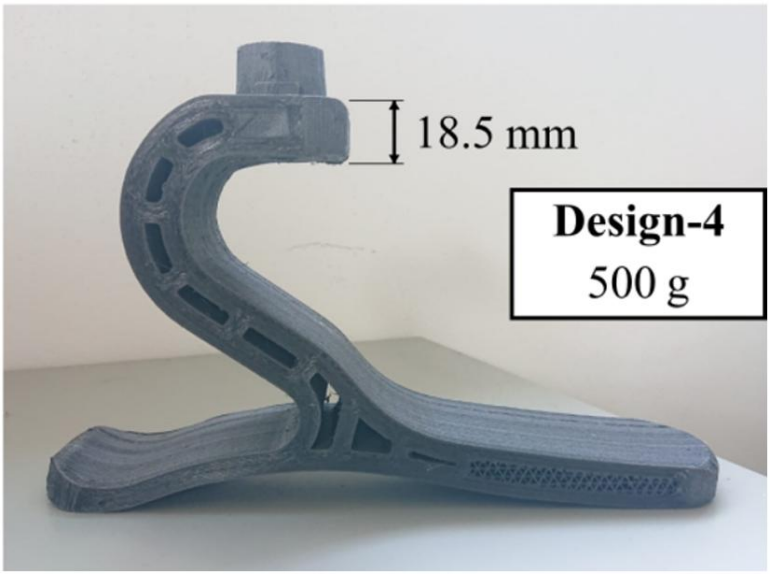

Figure 11: Prototype prostheses foot model.

Article published on 2024 [24] aimed to develop a numerical optimization tool to investigate potential designs for 3D-printed sandwich-structured composite foot prostheses as an alternative to laminated ones. A commercially available laminated prosthesis was analyzed to predict its stiffness behavior under various loading conditions which led to the definition of reference stiffness parameters for the designed 3D- printed prosthesis. Preliminary optimization considered weight as the cost function and was able to achieve two feasible solution. The obtained design demonstrated different stiffness behavior, when analyzed using plane stress finite elements. This was mainly due to the simplification considered in modeling geometry. However, the current tool only serves as a rapid and versatile approach for making preliminary design decisions. This published study focuses on Energy Storage and Return (ESAR) feet, produced by Continuous Fiber-Reinforced Additively Manufacturing (CFRAM) method.

In a study published in 2022 [10], a 3D-printable foot prosthesis (Figure 12) was designed and manufactured using PA12 material. The objective of this research was to develop an inexpensive prosthetic foot that was robust enough to carry out a variety

of tasks while being lightweight, flexible, and energy capable. Nylon PA 12 is hygroscopic, meaning it absorbs moisture from the environment over time, also may degrade when exposed to prolonged sunlight or UV radiation.

Figure 12: Nylon PA 12 foot.

In another study published in 2022 [11], proposed a new passive foot design (Figure 13) that is more energy efficient if 3D printed using thermoplastic polyurethane (TPU) material. TPU, being a flexible material with high strength and durability, is chosen as the material for the 3D printed foot. The analysis performed on the foot is for an 80 kg person at different angles during the gait cycle for the K2 human activity level. Main drawback in this foot is that it was not tested according to the ISO 10328: 2016, P5 level.

Figure 13: 3D printed TPU foot.

In the paper published in 2019 [12], The aim is to develop a methodology to design low-cost, short production-time prosthetic feet (Figure 14), with a natural-aesthetic, using 3D scan technology, CAD modelling and AM technology, able to improve the amputee's gait cycle. Both modelling and production of the prosthetic foot include two components: a rigid material (PLA) for impact absorption and pylon connection (internal); and a flexible material (Filaflex 82A) for energy dissipation and

better aesthetics (external). A 5-year-old bilateral amputee girl was the clinical case study. The foot is tested with 531N in three conditions – toe-off, heel-strike and mid-stance using both FEM analysis and experimental method. In this study the foot is not tested according to the ISO standards.

Figure 14: 3D printed TPU foot with rigid PLA on the interior.

Paper published in 2023 [26] studied the fatigue property of ABS specimen manufactured by fused filament fabrication method. The experimental fatigue assessment data provided the Basquin formulation along with values of constants 'A' and 'b' used in the formulation. This equation can be used in current study to estimate the fatigue life of the prosthetic foot design.

Finally, the study is performed in collaboration with Roadrunnerfoot Engineering s.r.l. The existing SACH foot is already tested experimentally by Roadrunnerfoot Engineering in three loading conditions namely toe-off, mid-stance and heel-strike. The experimental data for static is given in Table 1 below. A maximum load of 2240N is applied in static assessment and a cyclic load pulsating from 50N and 1500N is applied for the fatigue assessment respectively. These data are considered while designing the prosthetic foot.

Table 1: Static assessment experimental data from Roadrunnerfoot Engineering

	Max deflection (mm)
Toe-off	28
Heel-strike	40

Chapter Two

2. Material and Process selection:

Prosthetics are made lightweight for better convenience for the amputee. Wood, rubber, lightweight metals like titanium/aluminum, composites like carbon fiber, and different types of plastics are used in the manufacturing of prosthetics. Prosthetic feet are generally made by injection molding process. Injection molding is a traditional manufacturing technique, and it is used when at least 10,000 identical parts are required, otherwise it is very costly. The initial process to start the injection molding is complicated, takes a lot of time, requires skilled staff, and is costly. Once the process is established, the fabrication time of the part is reduced. With the rapid advancement in technology, additive manufacturing techniques are considered as an emerging solution for the fabrication of prosthetics [13].

The goal is to make a 3D printed passive prosthetic foot with similar kinds of properties as foot with injection molding. But there is major concern with this manufacturing technique that it is very difficult to predict the mechanical properties of 3D printed part and still there is no accurate methodology.

The mechanical properties of FFF 3D printed parts are solely dependent on printing setting parameters and environment conditions. The most significant setting parameters include percentage infill, nozzle speed, nozzle temperature, bed temperature, etc. A slight change in one of these parameters leads to different mechanical properties of same identical part printed from the same printer in identical environment. For example, varying the infill percentage and the dimensions of the 3D printed part will significantly vary its compressive and tensile properties [14]. In contrast, changing the nozzle and bed temperature leads to a change in rate of diffusion between the layers [15].

TPU 70A filament (FilaFlex from Recreus Industries, S.L. [22]) was the material of choice for the flexible part of the foot and ABS (Hyper ABS from Creality [23]) is chosen for the rigid part of the foot in this study. The material properties of the two materials are listed in Table 2.

Table 2: Material properties

	TPU 70A	ABS
Density (g/cm³)	1.08	1.04
Tensile strength (MPa)	32	27
Elongation at break (%)	900	7.63
Young's Modulus (MPa)	1.93 (estimated)	1975
Stress at 20% elongation (MPa)	1.5	-
Stress at 100% elongation (MPa)	3.5	-
Stress at 300% elongation (MPa)	6.3	-

In this study, the material model of TPU 70A is assumed to be linear elastic behaviour. To obtain the young's modulus of the material, the stress and strain data provided in the table is used. The slope of the linear trend line obtained from linear regression model indicates the young's modulus of the TPU 70A material. Therefore, from the chart (Figure 15) the young's modulus of TPU 70A is calculated as 1.93Mpa. FilaFlex is a thermoplastic polyurethane and Qi and Boyce [16] stated that for polyurethane (TPU) "it is reasonable to assume the Poisson's ratio ranges from 0.48 to 0.5". According to Tsukinovsky [17] and Elleuch [18] studies, an average of 0.48 should be used for the Poisson's ratio. Due to the lack of studies with this filament, it was considered isotropic for FEA simulations.

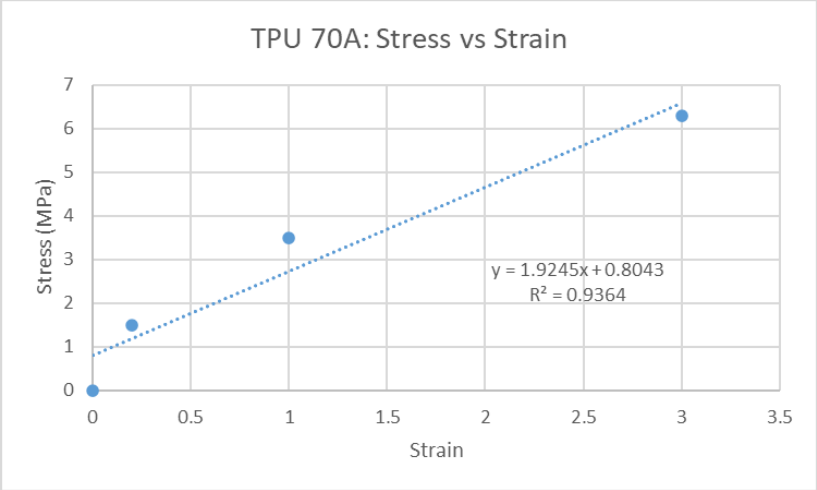

Figure 15: Stress vs strain of TPU 70 A.

2.1 Test Procedure:

The prosthetic foot is tested according to the ISO 10328: 2016 standard and P5 loading level [19]. During the following tests, the floor is maintained at an inclination of 20° (β) and 15° (α) with respect to horizontal plane for the toe-off and heel-strike conditions respectively (as shown in Figure 16). A load of 2240N is applied on the top surface of the pyramid connector.

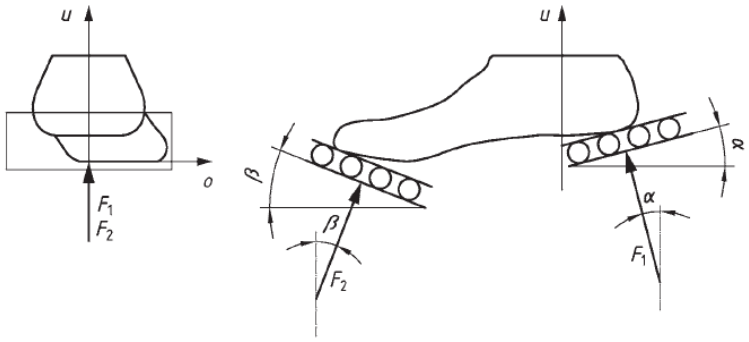

Figure 16: ISO 10328: 2016 test procedure.

- Static load test: A static load of 2240N is applied to the top surface of the prosthetic foot (top surface of the pyramid connector). The foot must sustain the load applied with no permanent deformation or with permanent deformation less than 5mm.
- Fatigue load test: After the static load test, the same prosthetic foot must be tested with the cyclic load of maximum 1500N and minimum 50N and the prosthetic foot must withstand minimum of $2x10^6$ cycles. Followed by a final static test with application of 2240N load. At the end prosthetic foot must withstand with no permanent deformation or with permanent deformation less than 5mm. Here, the maximum cyclic load of 1500N is applied instead of 1330N due to the requirement of Roadrunnerfoot Engineering company.

2.2 Finite Element Analysis of Prosthetic foot:

2.2.1 Simplified 2D analysis:

In this study, Finite element analysis is performed using Abaqus software. First the foot is analyzed with simplified 2D shape. Here only the foot is considered, and the screw and pyramid connector are not included in the 2D analysis. The foot is made up of TPU 70A material, while the floor is assumed to be steel material with young's modulus of 206GPa and Poisson's ratio of 0.33. Since the simulation is carried out on a 2D section, the force of 2240N has been converted to equivalent load of 65N. The

setup for toe-off (Figure 17), mid-stance (Figure 18) and heel-strike (Figure 19) conditions are shown below.

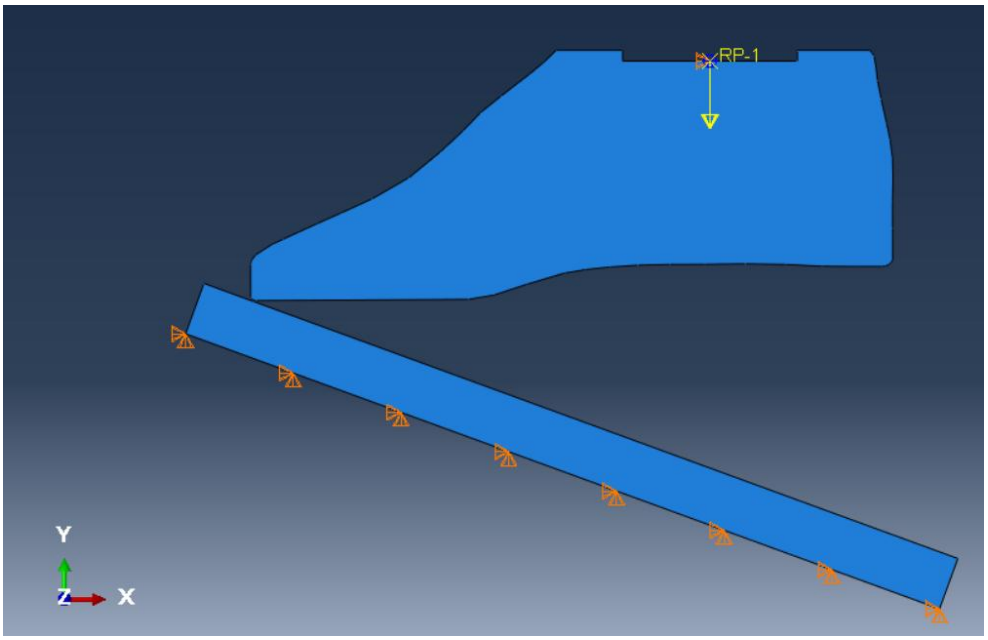

Figure 17: Toe-off condition in 2D analysis.

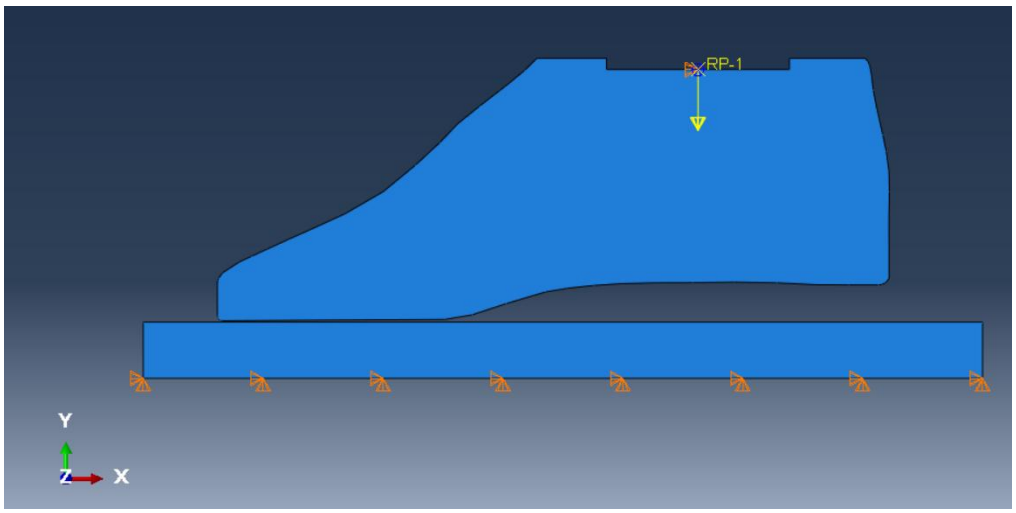

Figure 18: Mid-stance condition in 2D analysis.

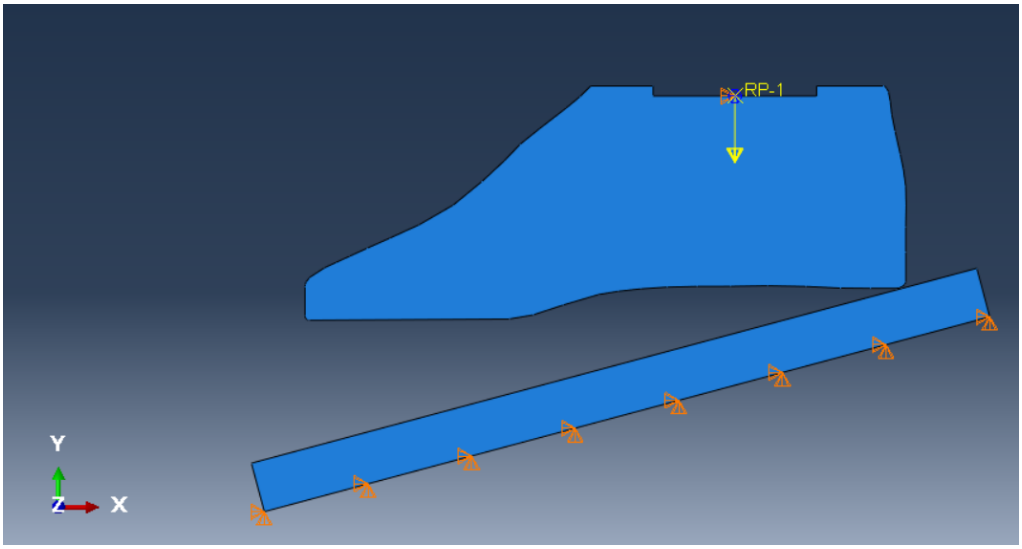

Figure 19: Heel-strike condition in 2D analysis.

2.2.2 Convergence analysis:

To assess the accuracy of results, it is necessary to apply convergence analysis techniques. The method is defined as "Zero Size Method" and it is based on a suitable mesh refinement method and an estimate of the error based on the order of the polynomials associated to the elements used. Polynomials are used to express the displacement fields.

Given, h, element characteristic length and p, order of the full polynomial included in the displacement field associated to the elements used. The discretization error, that measures the speed of convergence is proportional to:

- h^q where q = p+1 for the description of displacements
- h^q where q = p for the field obtained by differentiation (stress or strains)

The error, function of h^q, being q the order of the error for the quantity Φ, varies linearly with h^q (Equation 2.1) as shown in Figure 20, [20].

$$\Phi_\infty = \frac{\Phi_1 h_2^q - \Phi_2 h_1^q}{h_2^q - h_1^q} \tag{2.1}$$

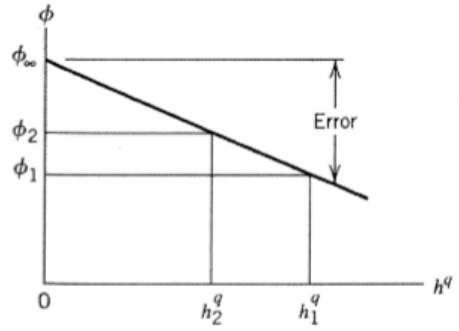

Figure 20: Plot showing Linear relation between quantity Φ and h^q.

In case of irregular mesh refinement, a dimensionless h can be defined by Equation 2.2 as

$$h = \frac{1}{\sqrt[n]{N_{elements}}} \tag{2.2}$$

With,

n = 2 for 2D elements

n = 3 for 3D elements

and a linear extrapolation over 3 points should be performed.

In this study, to determine the mesh size, the simulation is performed in mid-stance condition with three different global element size (2, 3 and 4mm). The element chosen for this 2D simulation is CPS4 - A 4-node bilinear plane stress quadrilateral. The data gathered from the simulations are listed below on Table 3. The convergence chart (Figure 21) is plotted between the h^q and the U-magnitude. The U-magnitude represents the maximum deflection along the negative y axis, of the reference point (RP) on which the load of 65N is applied. Through linear regression model, the U-magnitude for theoretical zero size mesh is estimated. The constant term in the linear regression equation which is equal to 34.86mm is the U-magnitude at theoretical zero size mesh. With this value the error percentage is calculated for each case.

Table 3: Convergence analysis data

Global element size	No. of elements (N)	1/sqrt(N) (h)	h^q	U-Magnitude (mm)	U-Magnitude at zero size mesh (mm)	Error %
2	3081	0.0180	5.84E-06	34.8595		-0.01%
3	1141	0.0296	2.59E-05	34.8144	34.864	-0.14%
4	790	0.0355	4.50E-05	34.7995		-0.19%

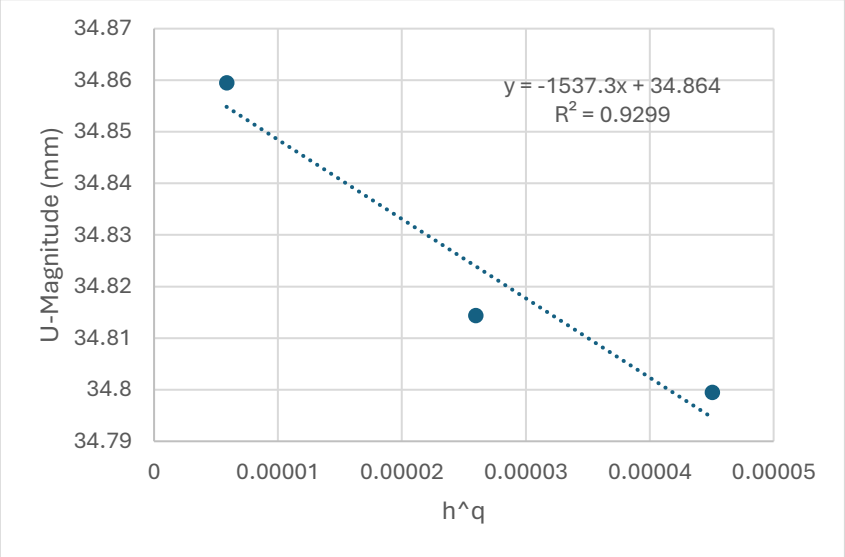

Figure 21: Convergence chart.

From the convergence analysis, it is estimated that for the global mesh size of 4mm, the percentage error in the displacement is 0.19% which is insignificant. This indicates that the mesh size of 4mm has sufficient accuracy in the results. Hence for this 2D simulation, a global mesh size of 4mm is used. The floor contact has a coarse mesh of 10mm.

Chapter Three

3. 2D Analysis Results:

The results obtained from the 2D simulation in three loading conditions – toe-off (Figure 22), mid-stance (Figure 23) and heel-strike (Figure 24) are shown below, where the left side of the figures indicates the von-mises stress induced in the material and the right side of the figure shows the deformation of the model due to the applied load mentioned in the previous section.

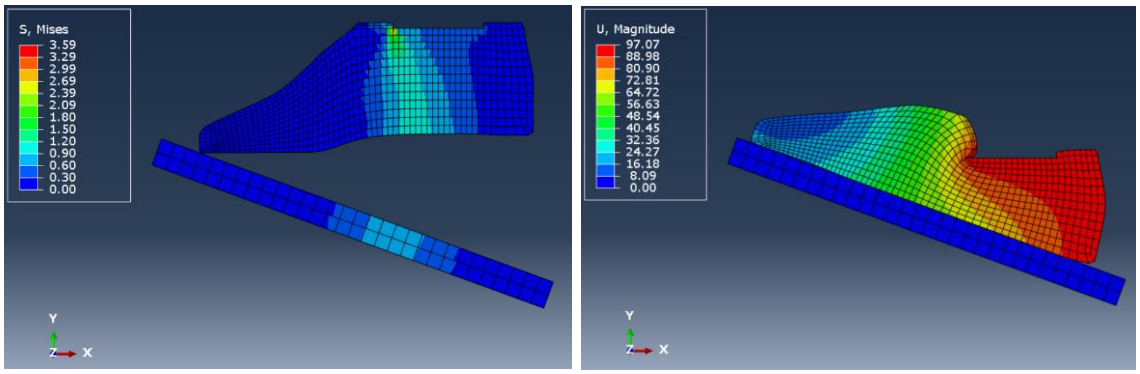

Figure 22: 2D analysis on Toe-Off condition.

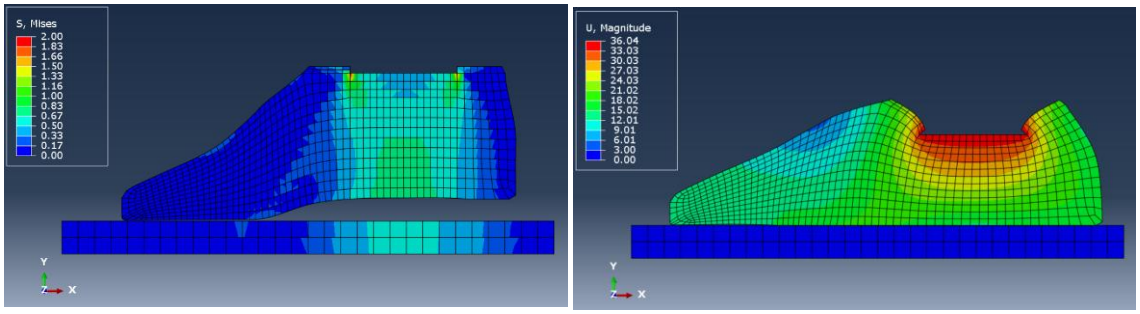

Figure 23: 2D analysis on Mid-Stance condition.

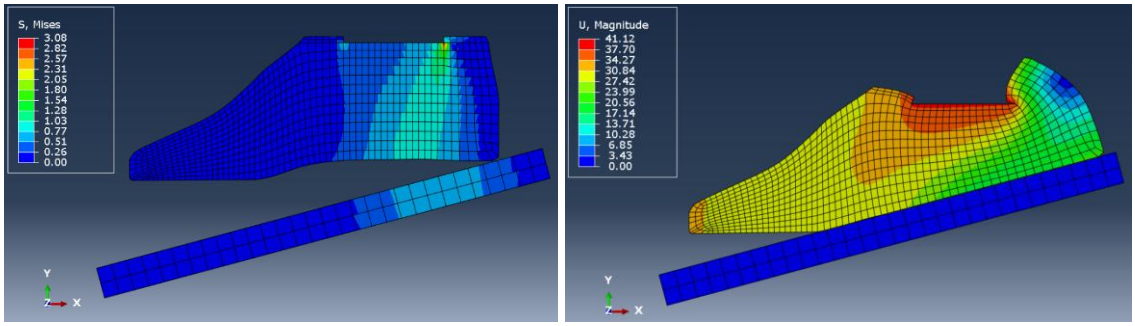

Figure 24: 2D analysis on Heel-Strike condition.

The displacement along vertical Y direction of the reference point (RP) are 94.05mm, 34.80mm, and 38.16mm for Toe-off, mid-stance and heel-strike loading conditions respectively. In this analysis, the force is applied on the reference point (RP) which is coupled to the top edge. Knowing the force applied on the RP point and its corresponding displacement it is easy to obtain the plot between force and displacement. The force vs displacement plots for toe-off (Figure 25), mid-stance (Figure 26) and heel-strike (Figure 27) loading conditions are below.

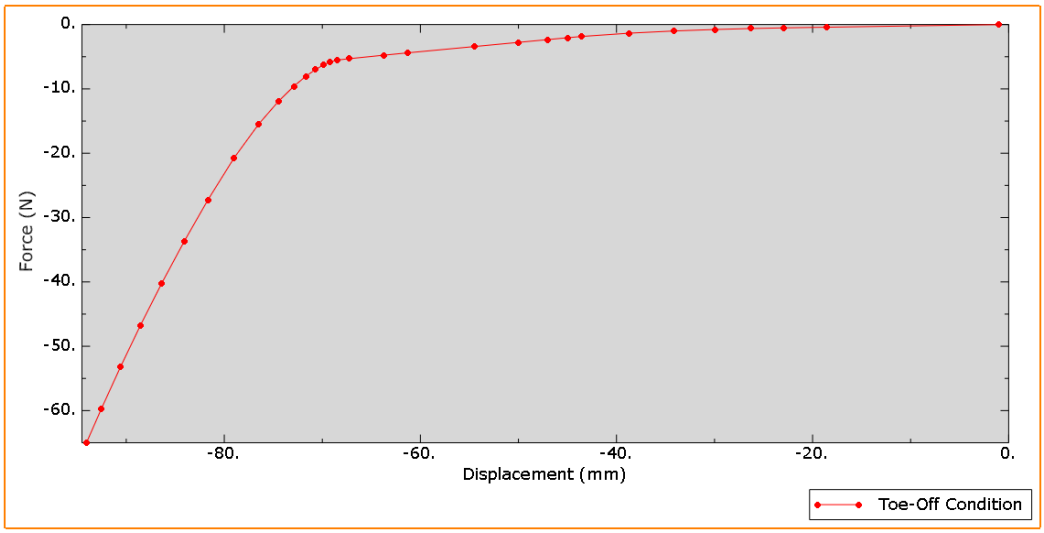

Figure 25: Force vs Displacement plot of Toe-off condition.

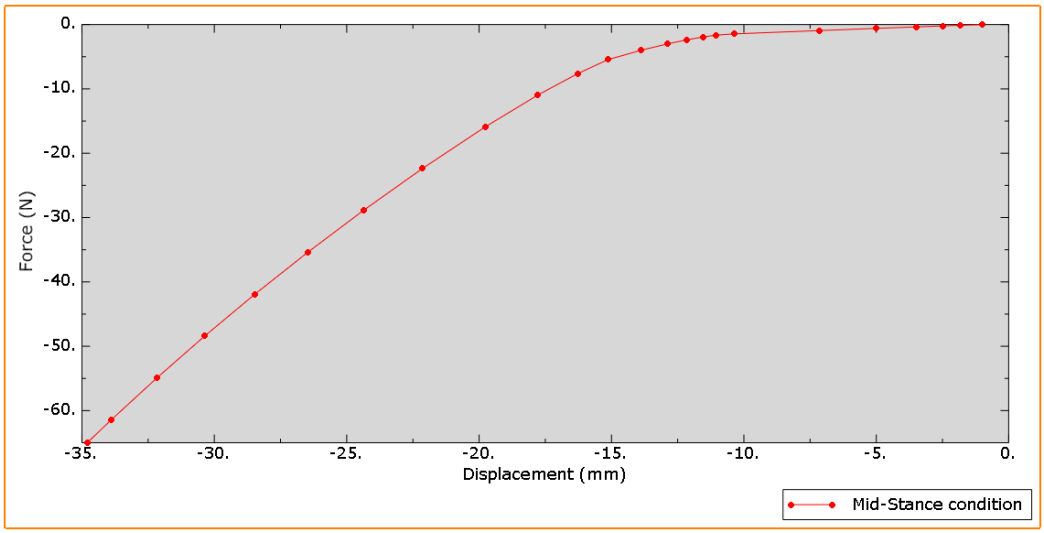

Figure 26: Force vs Displacement plot of Mid-Stance condition.

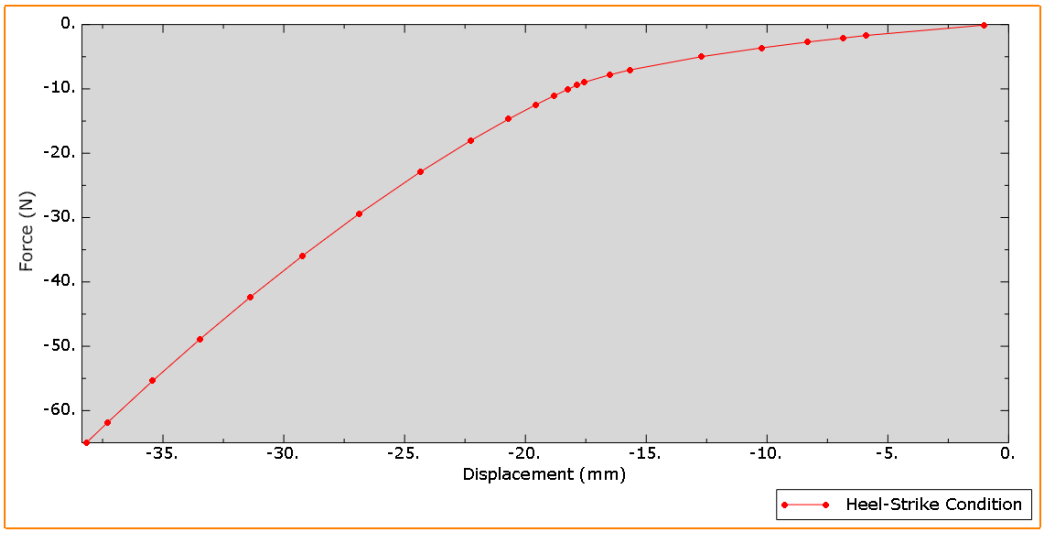

Figure 27: Force vs Displacement plot of Heel-Strike condition.

From the force vs displacement plots (Figure 25, Figure 26 and Figure 27) it can be understood that the stiffness of the foot is lower during the initial loading phase when compared to the final loading phase. Initially the foot undergoes bending until the base of the foot makes perfect contact with the floor surface, after that foot undergoes compression which leads to an increase in stiffness of the foot.

The 2D analysis indicates that the foot is highly flexible. The displacement in toe-off condition goes up to 97mm which is expected as the Young's modulus of TPU 70A is estimated to be 1.93Mpa which in turn makes the prosthetic foot less stiff. To increase the stiffness or reduce flexibility of the foot, either entire foot can be made of different material which has high young's modulus or add stiffer material inside the foot like presence of keel as in case of SACH foot. The keel material is usually stiffer and can function as the bones in our foot. In this study, it was decided to add an ABS

keel inside the TPU 70A foot to improve the stiffness of the prosthetic foot. To better understand the impact of adding the ABS keel, the next simulation is performed by adding a simple ABS keel profile within the TPU 70A material as shown in Figure 28 and this 2D model is tested under same toe-off condition as before.

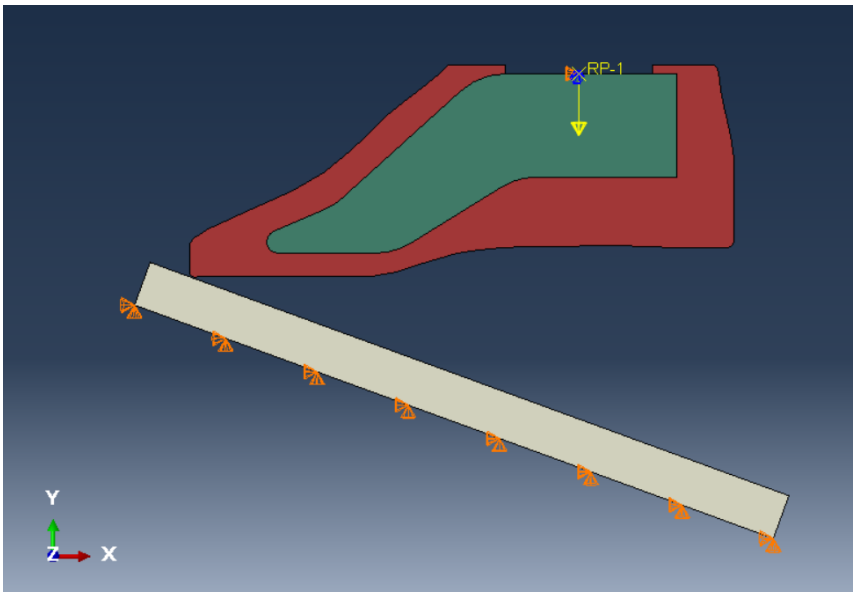

Figure 28: 2D Model with ABS keel (green) within the TPU 70A material (red) in toe-off condition.

The foot with keel is tested for the Toe-off condition. By comparing the force vs displacement plot for the prosthetic foot section without keel (Figure 29) and with the ABS keel (Figure 30), It is understood that ABS, which has high young's modulus (approximately 1000 times the young's modulus of TPU 70A material used in this study) increases the overall stiffness of the prosthetic foot. This is clear from the reduction in the displacement from 79mm to 19.4mm at the same load of 20.7N.

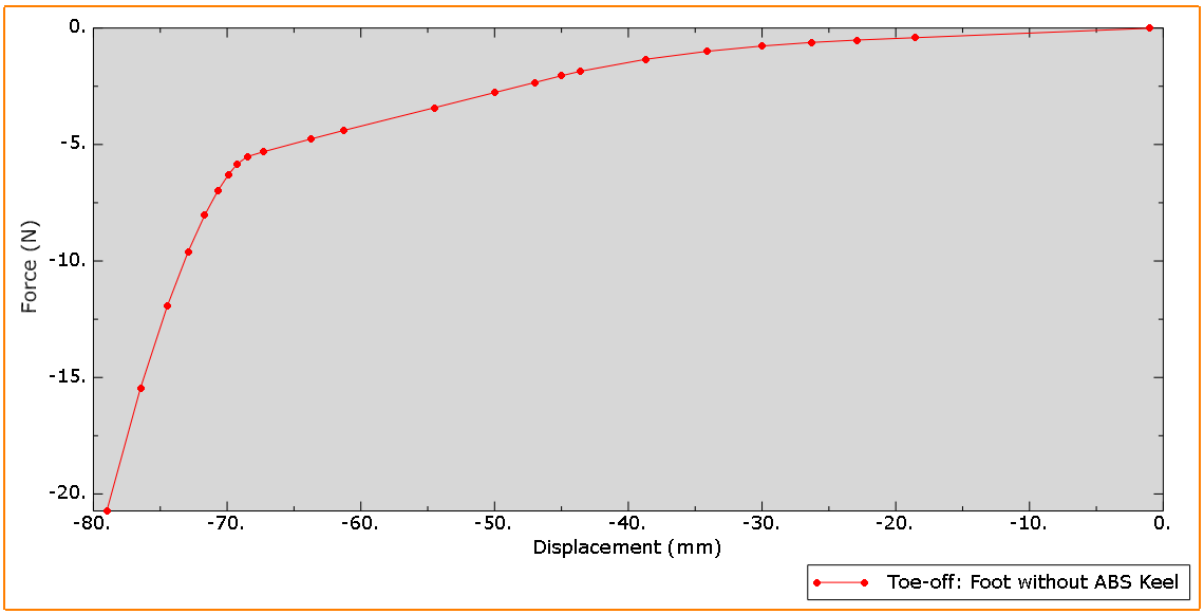

Figure 29: 2D Toe-off case without ABS keel.

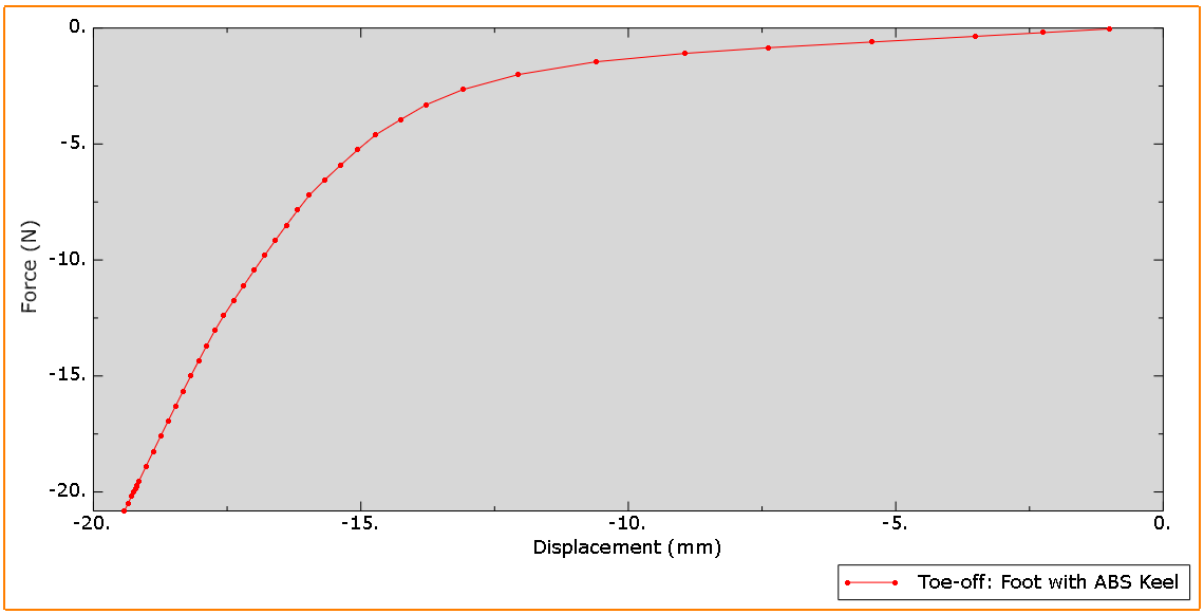

Figure 30: 2D Toe-off case with ABS keel.

Chapter Four

4. 3D Analysis of prosthetic foot:

The impact having ABS keel inside the TPU 70A foot is clearly understood from the previous study. Therefore, the prosthetic foot is designed with ABS keel surrounded by the soft TPU material. The prosthetic foot is made up of three components namely ABS keel, inner foot, and external cover. The inner foot and external cover are made up of the same TPU material. All the three above mentioned components are modelled in the CAD software – Solidworks 2024. The pyramid connector (Figure 34) and screw which helps in connecting the foot to the pylon are also included in the simulation. The pyramid connector and screw are the same components that is used by the company Roadrunnerfoot Engineering in their similar sized SACH foot. All the components that make up the prosthetic foot are converted into step files in the CAD software, which is then exported to Abaqus CAE software where the components are assembled. Material properties assigned to each component are given in Table 4, below.

Table 4: Material properties.

Components	Material	Young's Modulus (MPa)	Poisson's Ratio	Tensile strength (MPa)
Inner foot	TPU 70A	1.93	0.48	32
External cover	TPU 70A	1.93	0.48	32
Keel	Hyper ABS	1975	0.48	27
Screw	A2-70	196000	0.33	700
Pyramid connector	Aluminum 7075	72000	0.33	575
Floor (Assumed)	Steel	206000	0.33	-

The first step is determining the shape and size of the keel. The shape of the keel is determined by the traditional iterative process, first the analysis is started with a preliminary shape of keel as shown in Figure 31. The total length of this shorter solid keel is 215mm. The Inner foot (Figure 32), cover (Figure 33), pyramid connector (Figure 34), and screw along with the keel together are used in the 3D finite element model.

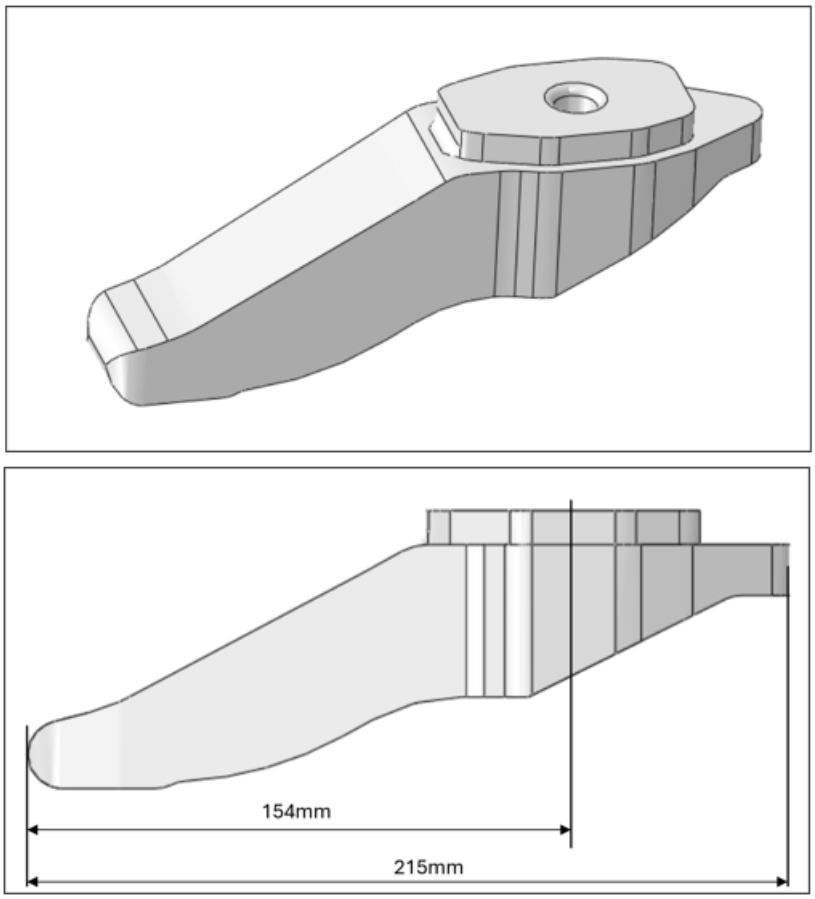

Figure 31: Shorter length keel used in first iteration with an overall length of 215mm.

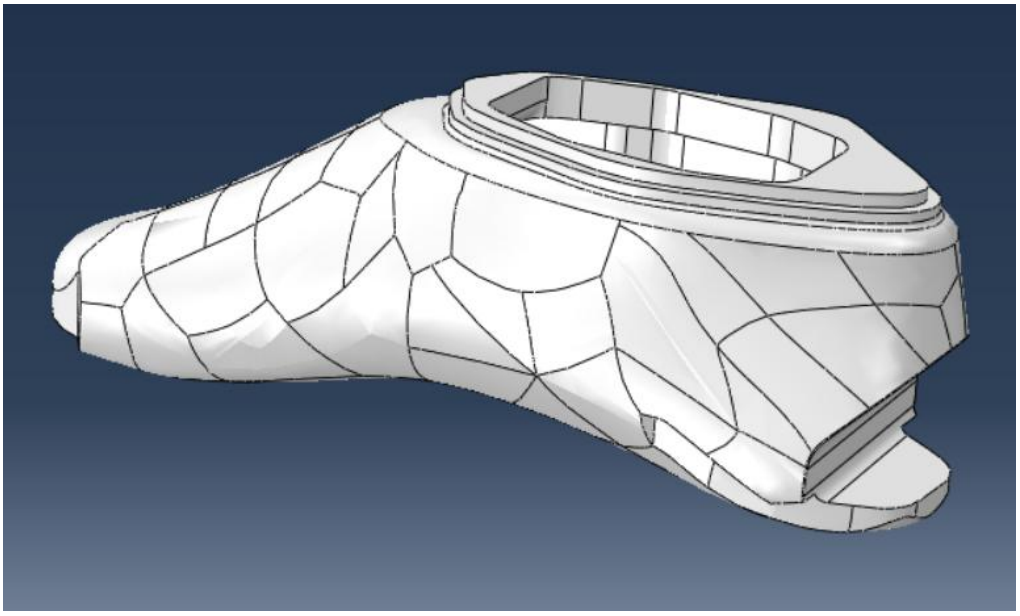

Figure 32: Inner foot.

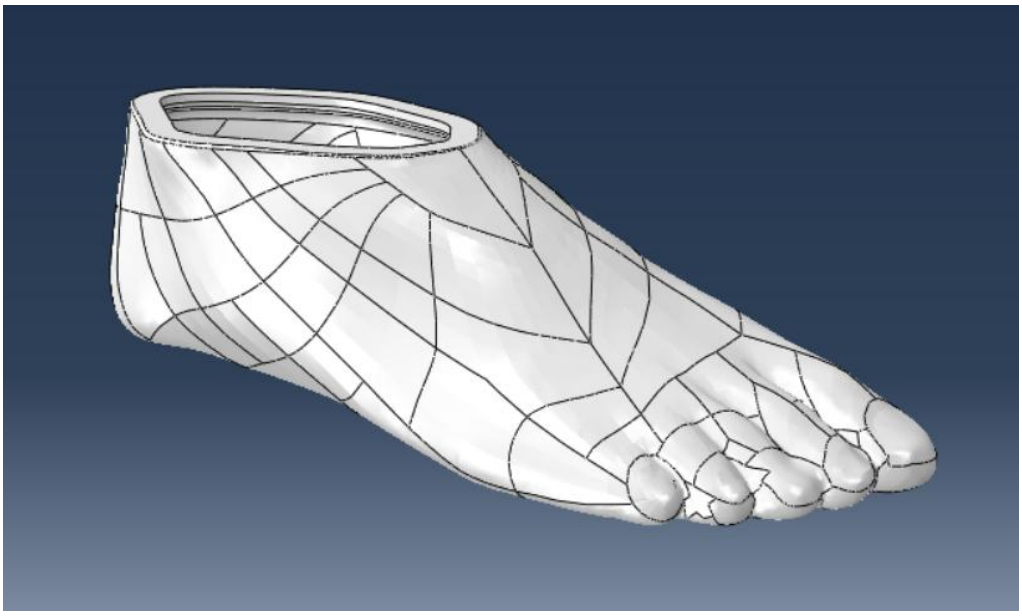

Figure 33: External cover.

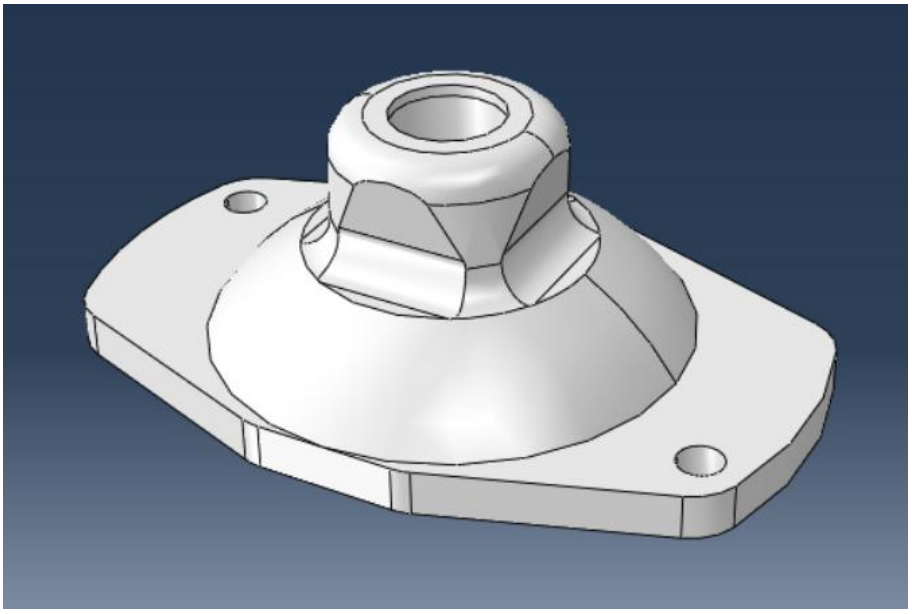

Figure 34: Pyramid connector.

The Above components are assembled as shown in Figure 35 for the toe-off loading case where the floor is inclined at an angle of 20° with respect to the horizontal plane. Figure 36 shows the cross-sectional view of the assembled prosthetic foot in toe-off loading condition with different colors indicating different components that make up the prosthetic foot.

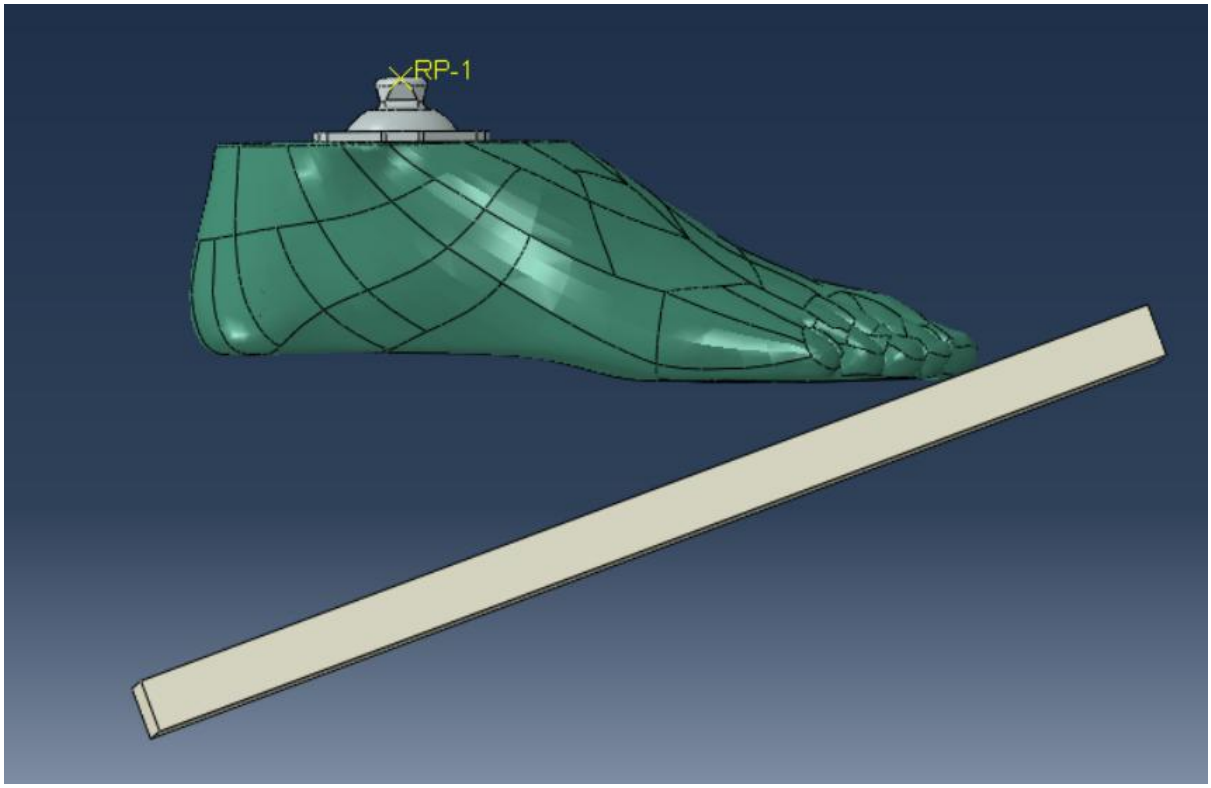

Figure 35: Prosthetic foot assembly in toe-off case. Floor inclined at angle 20°.

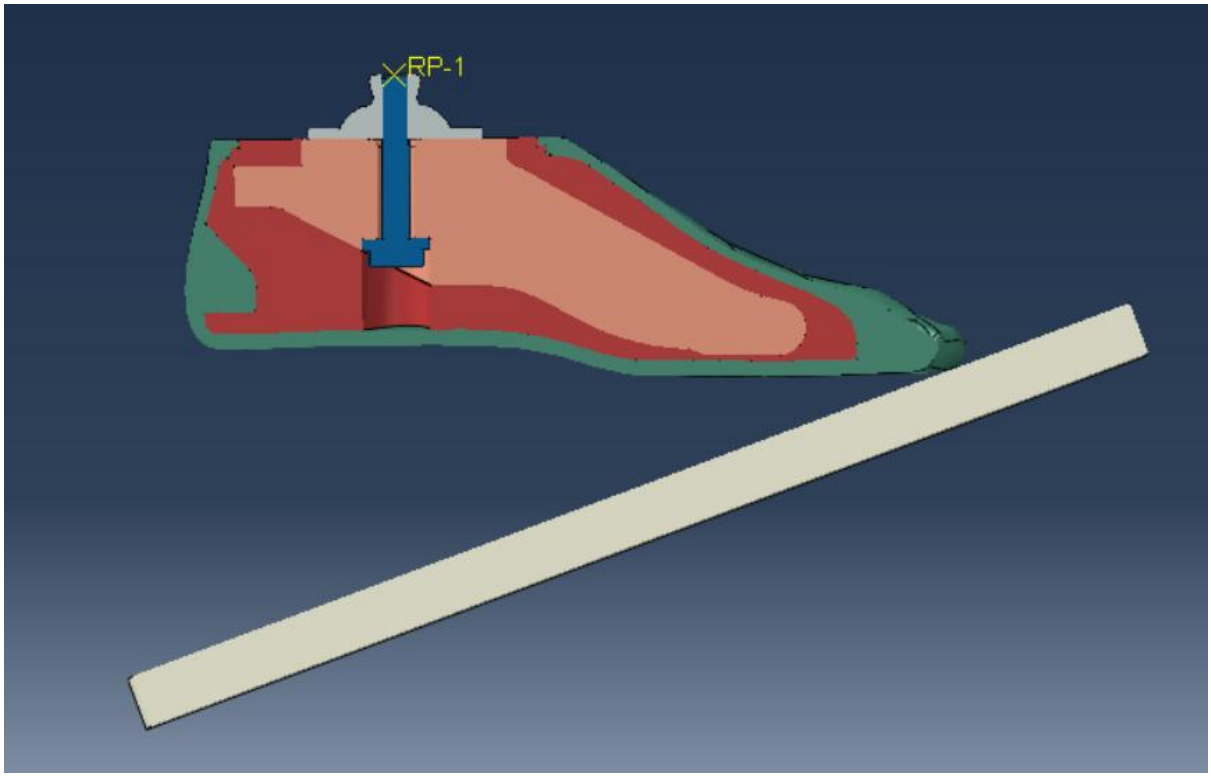

Figure 36: cross-section in toe-off loading condition showing cover (green), inner foot (red), shorter length solid keel (pink), screw (blue), pyramid connector (grey) and floor contact (white)

The next crucial step in this study is to add interactions between all the contact surfaces. The following interactions are added in this study,

1. Surface to surface interaction between floor and external cover.
2. Surface to surface interaction between external cover and inner foot.
3. Surface to surface interaction between keel and screw.
4. Surface to surface interaction between keel and pyramid connector.
5. Tie connection between inner foot and keel.
6. Tie connection between screw and pyramid connector.

In case of surface-to-surface interactions mentioned above, Main and secondary surfaces are assigned according to the set the rules given below [20],

1. The large of two surfaces must act as the master surface.
2. If the surfaces are of comparable size, the surface on the stiffer body should act as the master surface.
3. If the surfaces are of comparable size and stiffness, the surface with the coarser mesh should act as the master surface.

In each surface-to-surface interactions, the sliding formulation is chosen to be finite sliding, surface to surface discretization method and auto adjustment option is enabled to remove any initial penetration of surfaces since the components are imported as step file inside the Abaqus software, the surfaces may not be smooth as viewed in the CAD software. Each surface-to-surface interactions are assigned with tangential and normal behaviour. In case of tangential behaviour penalty friction formulation is used with a frictional coefficient and that in case of normal behaviour, hard contact pressure-overclosure method and penalty constraint enforcement method are used. Also, here the surfaces are assumed to be inseparable after contact. A non-linear contact stiffness behaviour is also used.

The simulation is of two steps. During the first step preload, a displacement of 2mm is given to the Reference point (RP) which is coupled to the top surface of the pyramid connector. This is to ensure that all the contact surfaces are in contact before applying the load in the next step. The second step is when the load of 2240N is applied to the RP. The loading and boundary conditions for toe-off (Figure 37), mid-stance (Figure 38) and heel-strike (Figure 39) conditions are shown below. In any case, the floor bottom surface is fixed, and all the displacement and rotation of RP are constrained except the displacement in the vertical direction.

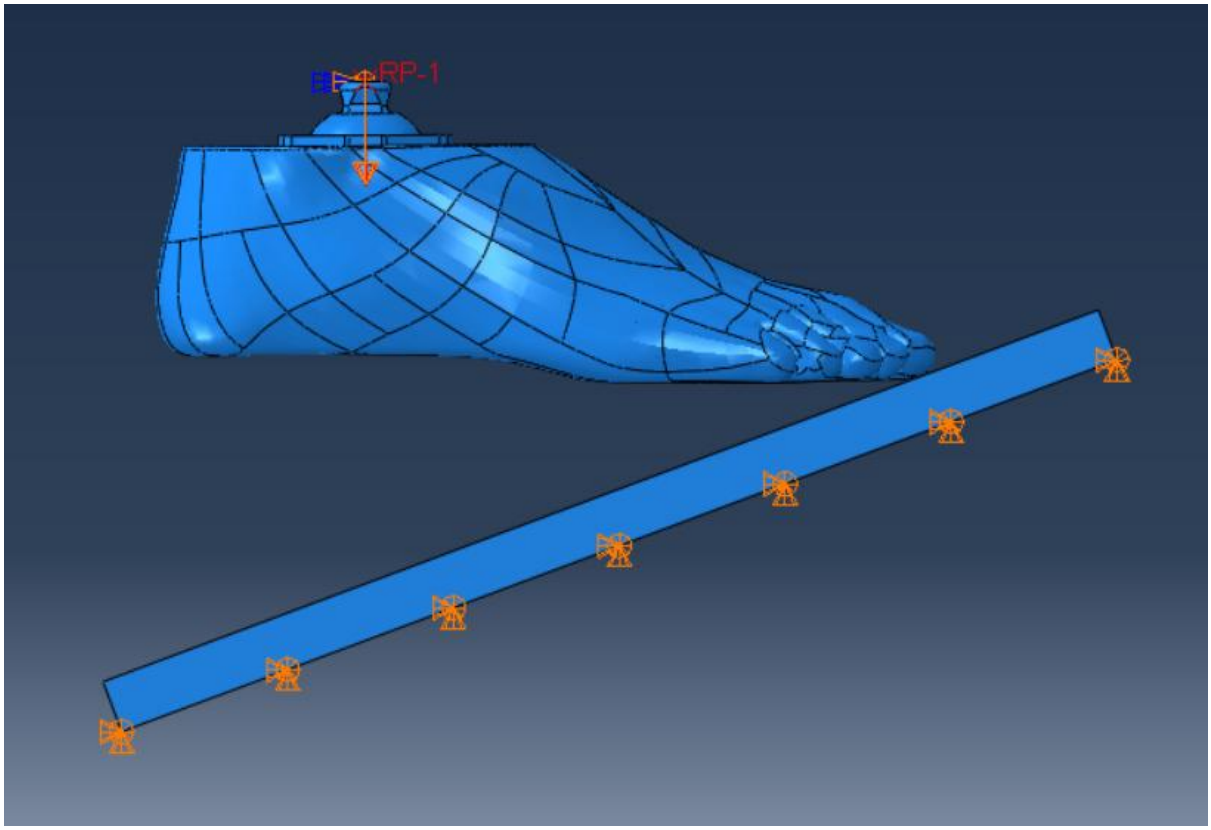

Figure 37: Boundary and loading condition in toe-off case.

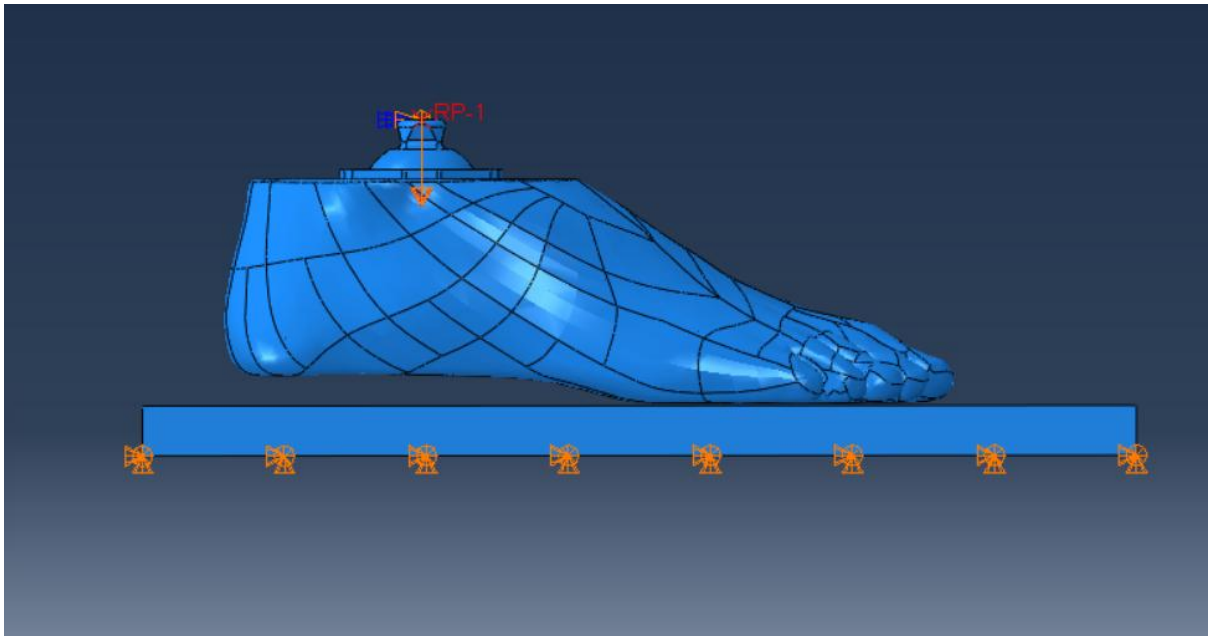

Figure 38: Boundary and loading condition in Mid-stance case.

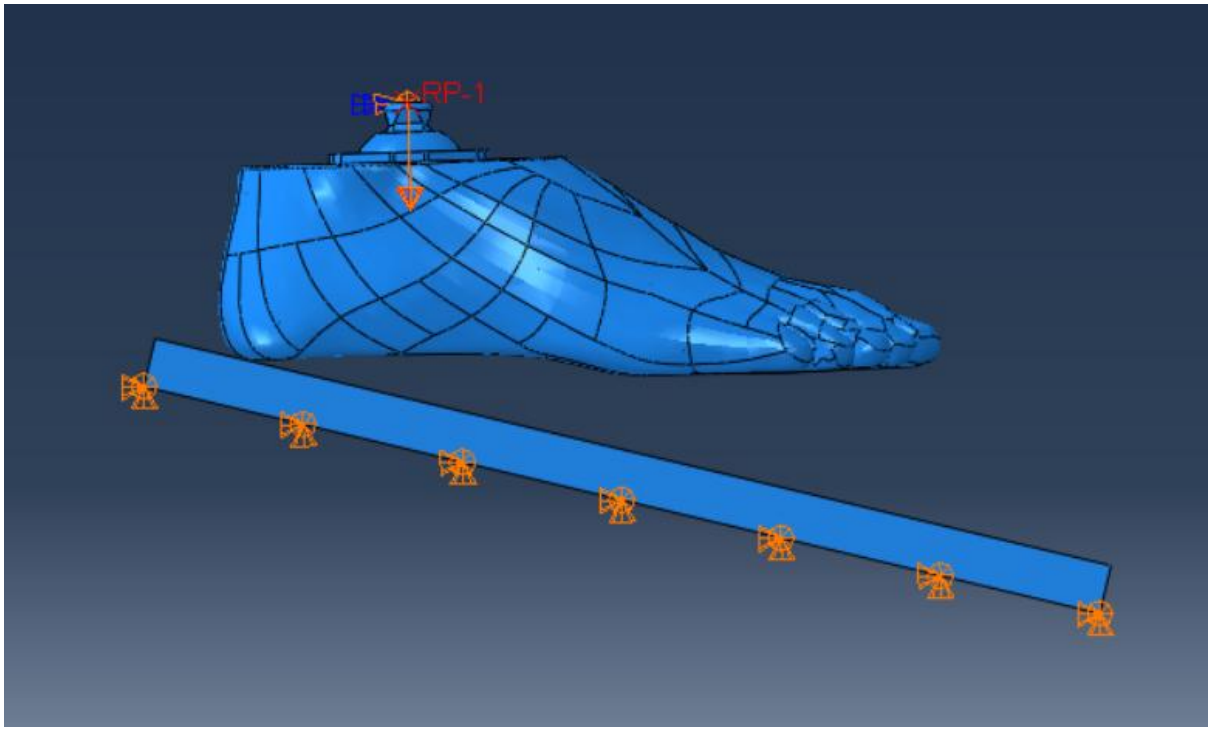

Figure 39: Boundary and loading condition in heel-strike case.

The components are meshed with a 4-node linear tetrahedron elements, C3D4. The components containing master and secondary surfaces are meshed in such a way that the master surface contains coarser mesh compared to its corresponding secondary surface. A total of 55,419 nodes and 240,952 elements are created at the end of the meshing process. These linear tetrahedral elements are chosen since the geometry is too complex to be partitioned to apply hexahedral elements.

The keel shape shown in Figure 31 is then tested in the toe-off condition with full load of 2240N according to the ISO standard mentioned in chapter 2 for the static loading. The results obtained are shown in Figure 40. The maximum deflection from now on will be considered as the value measured at the reference point (RP) for easy comparison. The results indicate that the maximum deflection was 28.6mm measured at the reference point (RP), which exceeds the experimental value provided by the Roadrunnerfoot Engineering company. Making the keel length shorter that this will result in lower stiffness and thus higher maximum deflection. Hence for this reason, the keel is made longer by 26mm. The new keel which is now called as longer length solid keel (Figure 41) has an overall length of the keel is 241mm. The second iteration is with this new solid keel which is again tested under the same loading and boundary condition for the toe-off case and the results are shown in Figure 42. The maximum deflection obtained in second iteration is 23.1mm, which can be seen in Figure 42, and is below the experimental value. Once the overall shape is fixed, then it is proceeded with minimizing the volume of the keel, thereby reducing the weight. Reducing volume is directly related to the stiffness of the model, therefore, reducing the volume

will lead to an increase in maximum deflection compared to that achieved in second iteration.

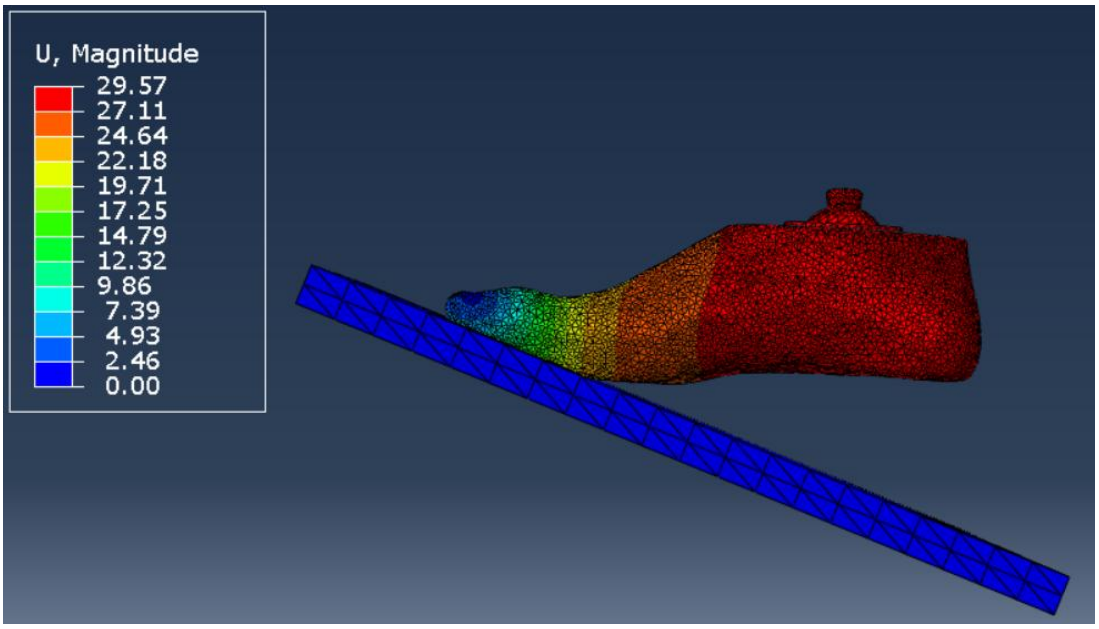

Figure 40: Maximum deflection in toe-off case with shorter keel used in first iteration.

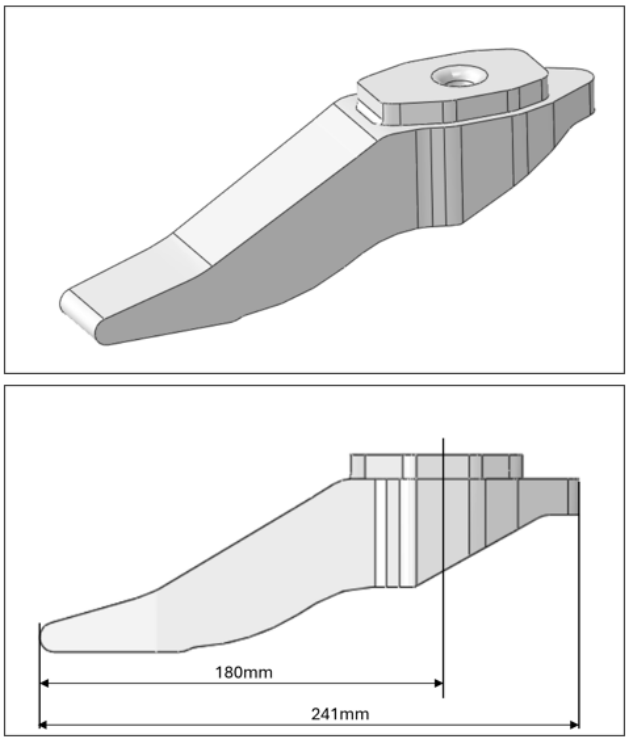

Figure 41: Longer length keel used in second iteration with an overall length of 241mm.

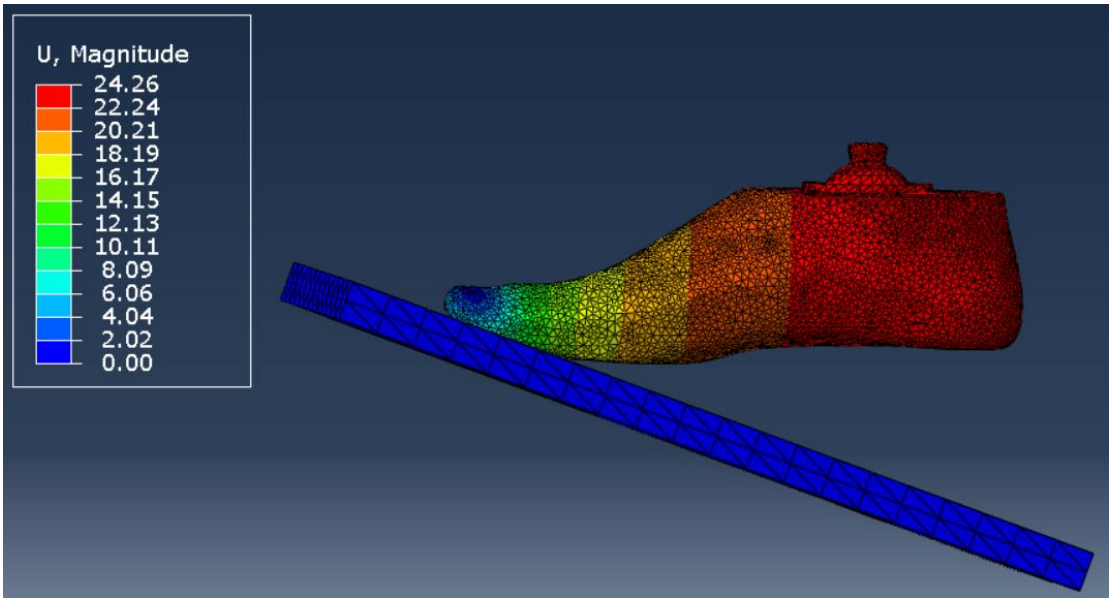

Figure 42: Maximum deflection in toe-off case with longer length keel used in the second iteration.

The results obtained from the longer length solid keel tested in toe-off case served as the starting point in minimizing the volume of the keel. The keel can be seen as two regions, namely A and B as shown in Figure 43. Region A is only influenced by the toe-off loading condition. From the second iteration, it is understood that in region A, the stresses are maximum at the top and bottom surfaces. The interior region has very minimal stress which is negligible compared to the values obtained in the top and bottom surfaces. The depth from top and bottom surfaces at which the stress becomes negligible is approximately 12mm. This depth is marked by red arrows in Figure 44.

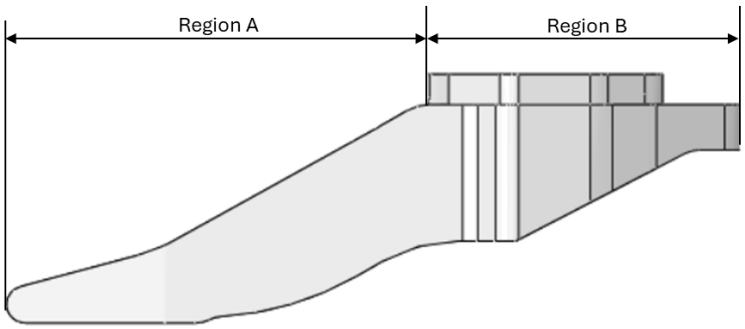

Figure 43: Keel divided into two regions A and B.

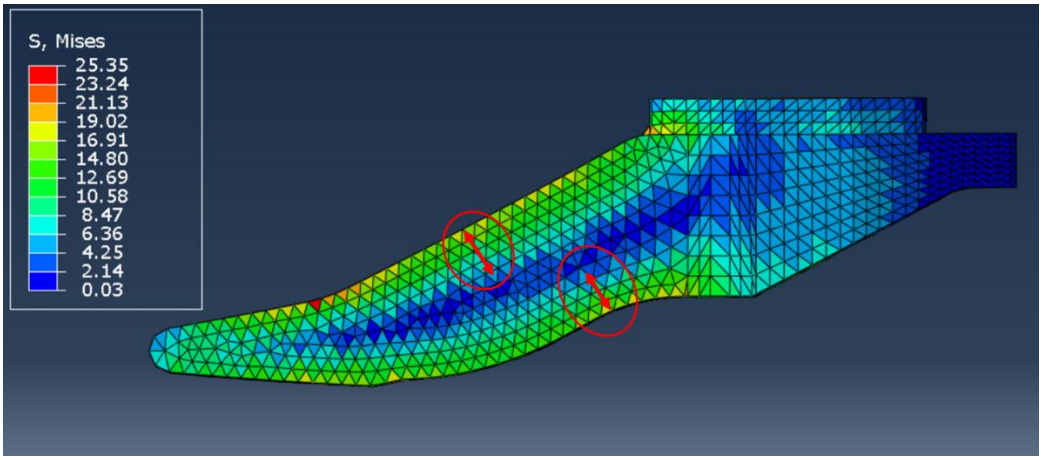

Figure 44: Variation of stress along the depth in keel.

The third iteration is done with the keel as shown in Figure 45. The top and bottom side have a 12mm thick layer, and the interior region is made hollow. Some ribs which are 5mm in thickness are added for additional support. This keel geometry is then tested with the same toe-off condition with the same load of 2240N. The results obtained are shown in Figure 46. The maximum deflection obtained using this new keel is 23.8mm and the maximum von mises stress obtained is 25.6Mpa. The deflections are lower than the experimental value provided by the Roadrunnerfoot Engineering company. Additionally, the stress induced is also lower than the UTS of the ABS material.

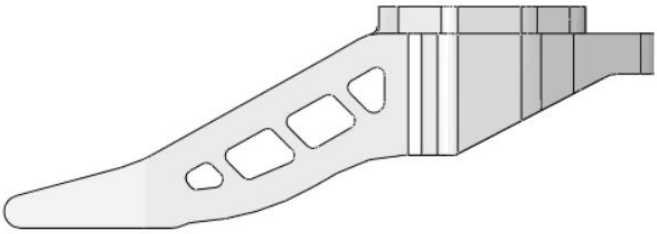

Figure 45: Keel with cuts in region A used in third iteration.

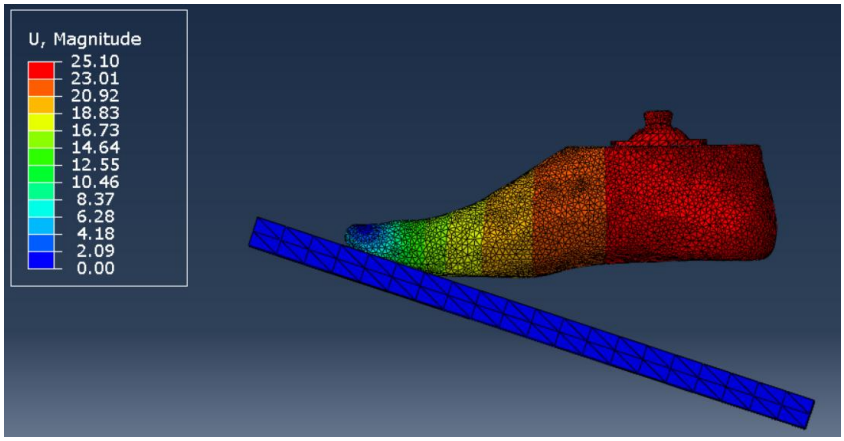

Figure 46: Maximum deflection obtained in third iteration.

Region B of the keel geometry is designed with a uniform wall thickness of 3mm (as shown in Figure 47) and was tested with the heel-strike conditions. In this case the stress induced is lower compared to the toe-off case. Moreover, the maximum deflection in the heel strike condition is influenced by the TPU material as the volume of TPU is higher than the ABS in this rear part of the foot. Therefore, the volume of the inner part of the foot is considered critical and thus it is minimized as much as possible. In the process to minimize the volume of the inner part of the foot at the rear end of the prosthetic foot, the hollow keel (Figure 47) is used. In the first iteration to minimize the volume of the inner part, first it is designed as a completely solid part and tested in the heel-strike condition with a load of 2240N as shown in Figure 48. Since the TPU material assumed to have a Poisson ratio of 0.48, it behaves like a nearly incompressible material. This is evident with the result (Figure 48) that is obtained from FEM analysis. The maximum deflection is 19.4mm which is less than the target value, but the heel portion of the foot seems more rigid. To make the rear part of the prosthetic foot more flexible, a cut is made on the inner part as shown in Figure 49. With this new geometry the second iteration is tested in the heel-strike condition. The results obtained (shown in Figure 49) from the analysis indicate that there is an increase in maximum deflection when compared to the first iteration. A third iteration is performed, in which additionally two more cut outs are made on the inner part as shown in Figure 50, which is then tested with the same conditions as before. With this design, the maximum deflection is 25.8mm as shown in Figure 50. The shape can further be optimized, but that is left for future work.

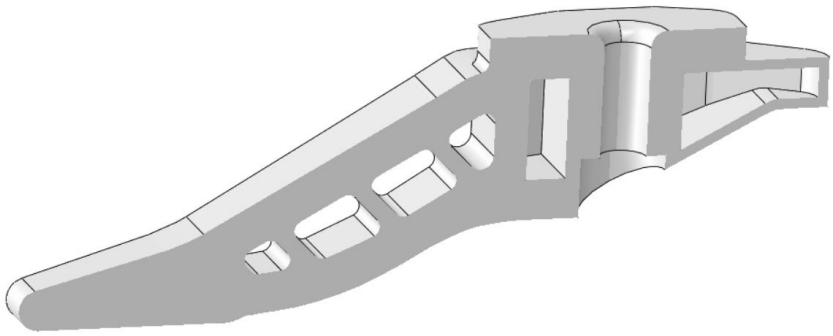

Figure 47: Final shape of Keel.

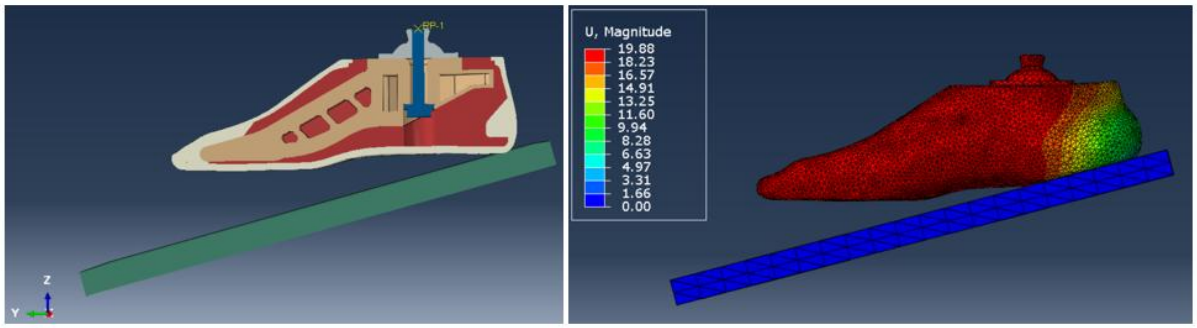

Figure 48: Assembled prosthetic foot with solid inner foot in heel-strike condition (left) and maximum deflection obtained in first iteration for inner foot (right).

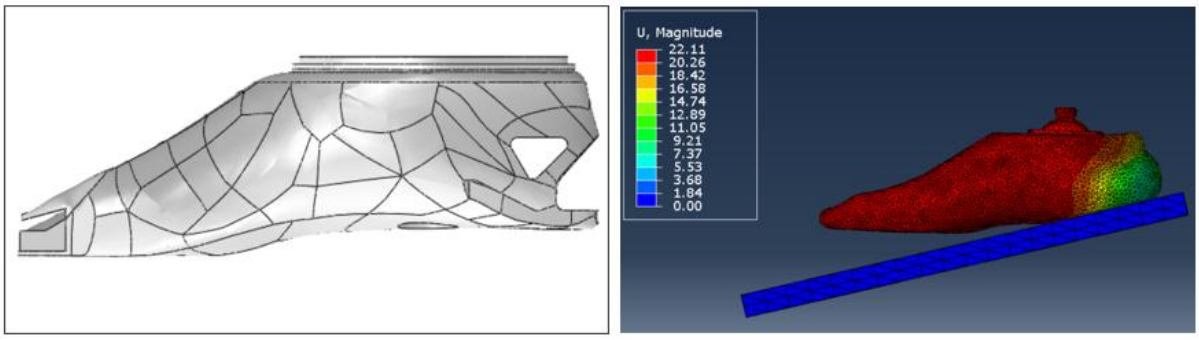

Figure 49: Inner foot with one through cut (left) and maximum deflection obtained in second iteration for inner foot (right).

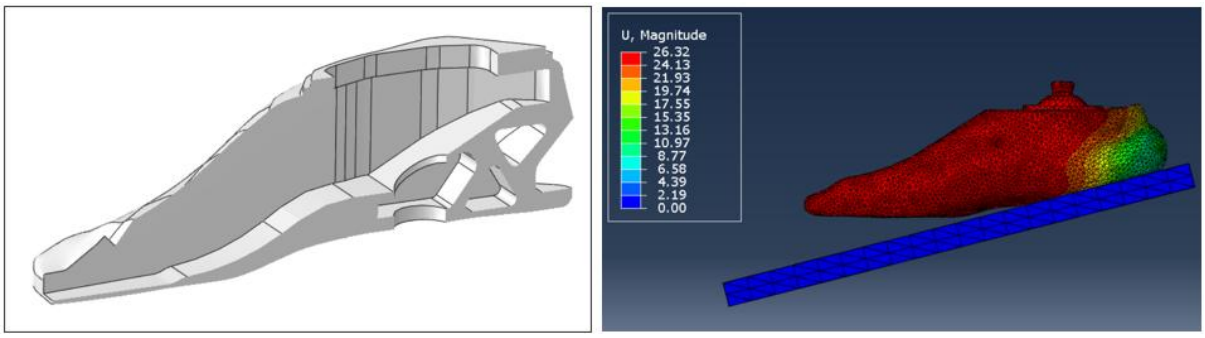

Figure 50: Inner foot with three cuts (left) and maximum deflection obtained in third iteration for inner foot (right).

At the end of these iterations, the final shape or geometry is decided for the inner part, cover and keel. The final design of Inner foot (Figure 51), cover (Figure 52), keel (Figure 53), pyramid connector (Figure 54) and screw are shown in the following figures.

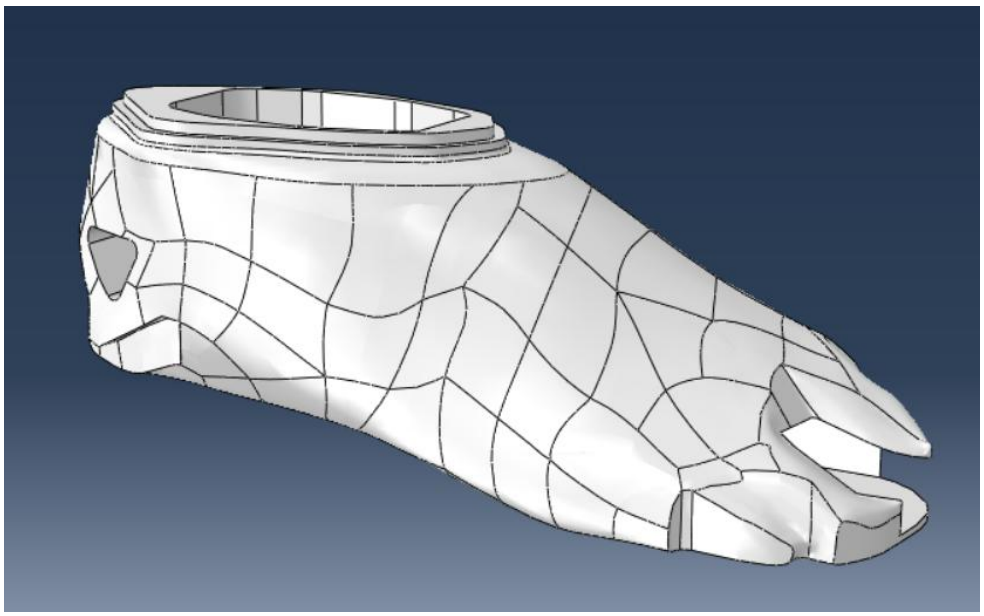

Figure 51: Inner foot.

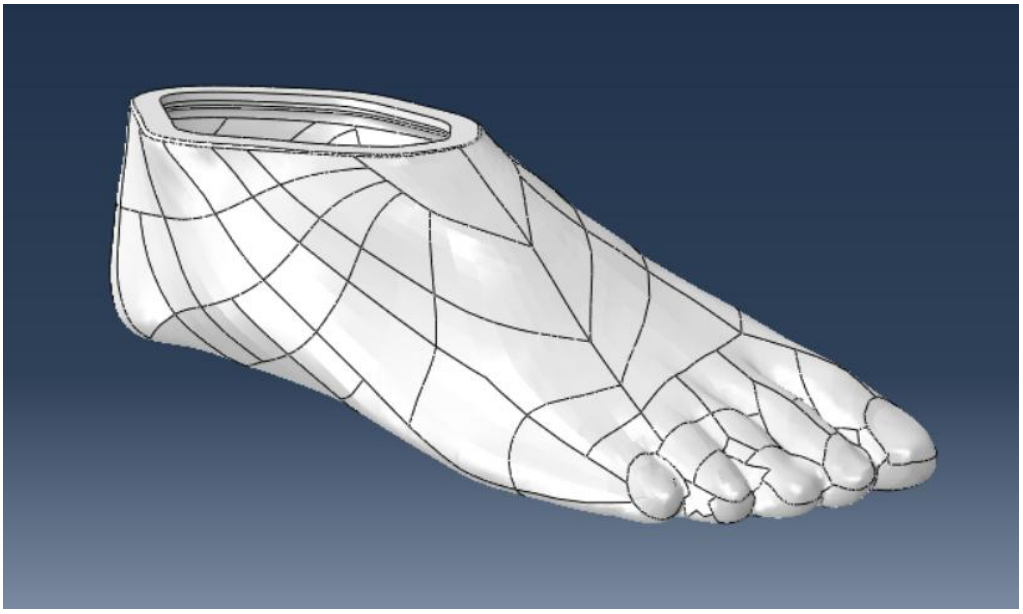

Figure 52: External cover.

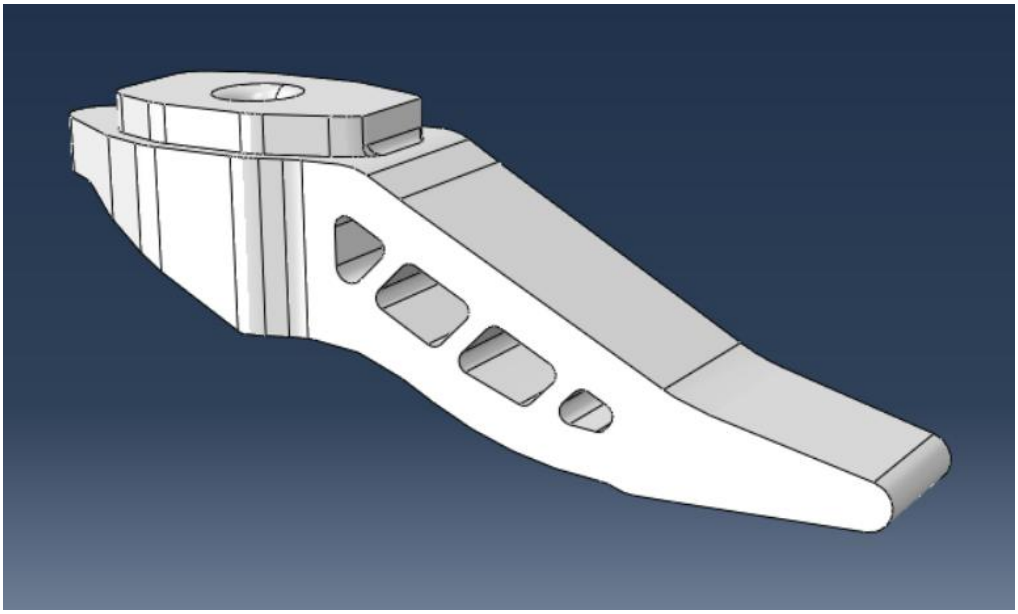

Figure 53: Keel.

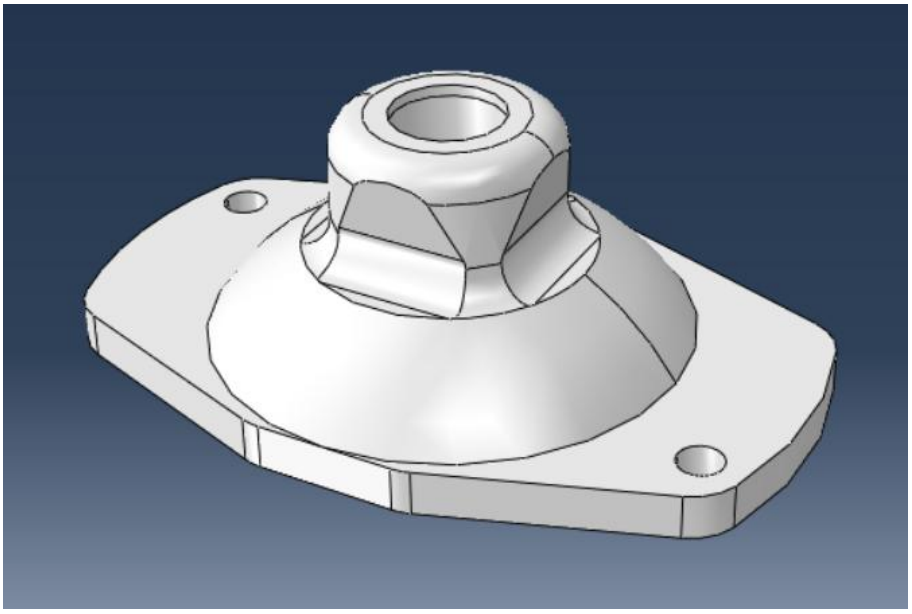

Figure 54: Pyramid connector.

All the components that make up the prosthetic foot are converted into step file in the CAD software, which is then exported to Abaqus CAE software where the components are assembled as shown previously to be tested in toe-off (Figure 37), mid-stance (Figure 38) and heel-strike loading (Figure 39) cases.

Chapter Five

5. Results of 3D analysis

The results obtained from the Finite element analysis of 3D model are shown below for the loading condition toe-off, mid-stance, and heel-strike respectively. The floor surface is inclined with respect to horizontal planes at an angle of 20° and 15° for toe-off and heel-strike loading conditions respectively. This is in accordance with the ISO testing standard mentioned in previous sections.

5.1 Toe-off case

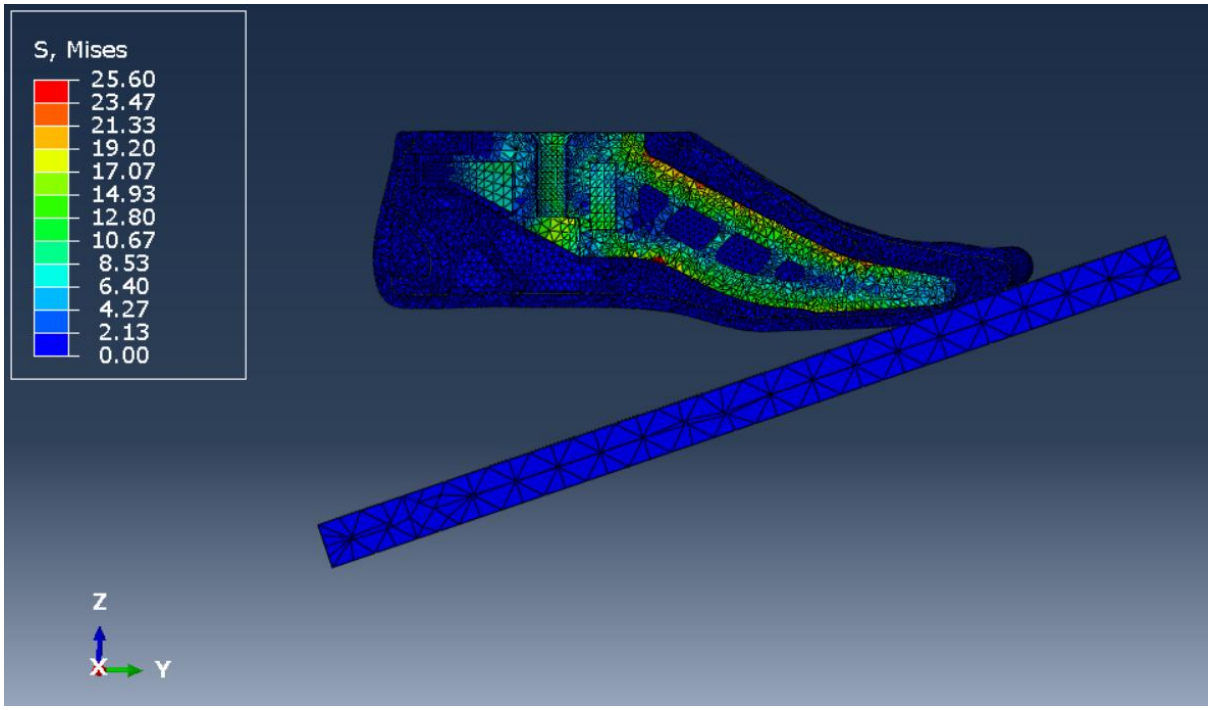

Figure 55: Von Mises stress of prosthetic foot (excluding screw and pyramid connector).

The von mises stress induced in the prosthetic foot (excluding the screw and pyramid connector) is shown in Figure 55 where the von-mises stress in the cover and inner

foot components are in the range of 0 to 2MPa which is clear from the blue color assigned to the elements of cover and inner foot while keel elements are assigned with color corresponding to the range above 6 to 8MPa. To get the clear value of stress in TPU components (inner foot and cover), the keel is excluded from the result (Figure 56) so that the von-mises stress range is only up to the maximum stress in the TPU components. The maximum stress induced in TPU components (inner foot and cover) are around 2MPa.

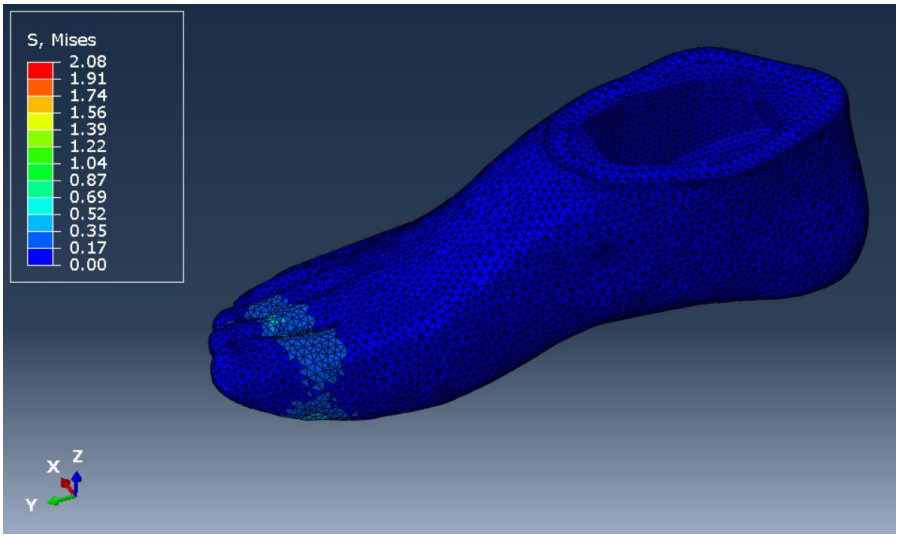

Figure 56: Von Mises stress of TPU components (inner foot and external cover).

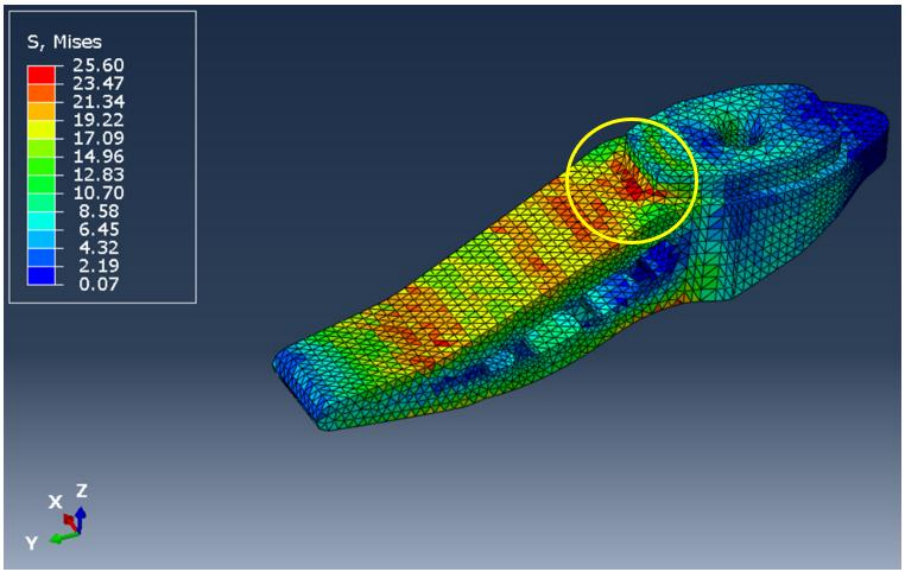

Figure 57: Von Mises stress of ABS Keel. The yellow circle showing location of maximum stress induced.

The results indicate that ABS keel is most stressed compared to the TPU components as TPU material has a very low young modulus compared to ABS. In

keel, the maximum stress of 25.6MPa is induced in corner region indicated by the yellow circle in Figure 57. Adding a higher radius to make smooth transition of flow from one region to another can help in reducing the stress induced. Region A experience higher stress than region B, this is due to nature of loading. In the toe-off case, the keel undergoes bending while region B undergoes minor compression at the final stage of loading phase, hence the stresses in region A are higher than region B as this is evident from the result shown in Figure 57. The deformation of the prosthetic foot under the applied load can be seen in Figure 58.

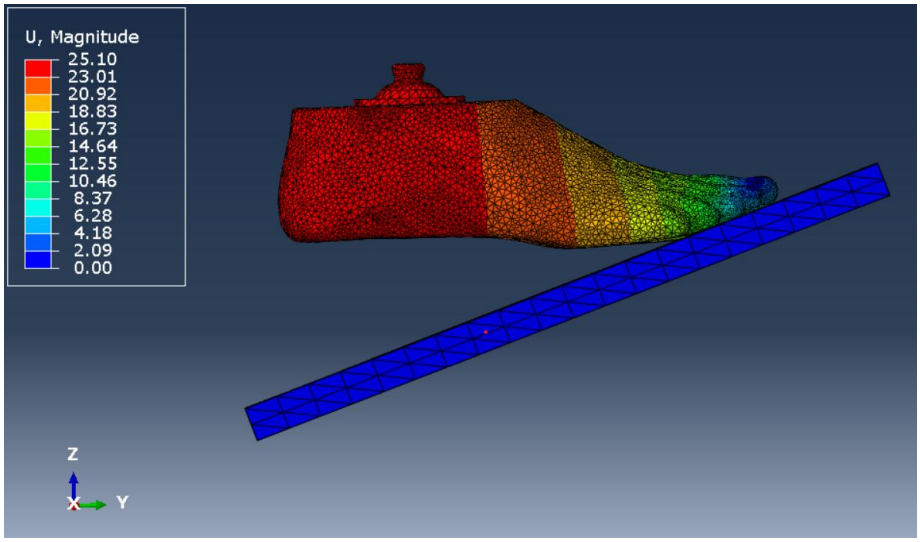

Figure 58: Deformation of prosthetic foot under applied load.

5.2 Mid-stance case

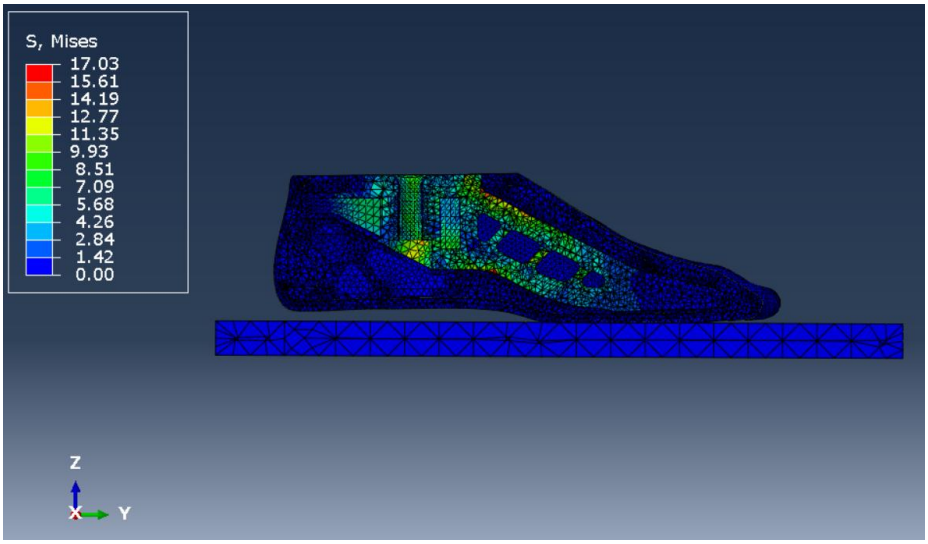

Figure 59: Von Mises stress of prosthetic foot (excluding the pyramid connector and screw).

By looking into Figure 59, which shows von-mises stress induced in TPU components (inner foot and cover) and keel, the stress induced in TPU components are in the range of 0 to 1.4MPa. By excluding the elements assigned to keel from the result view as shown in Figure 60, the maximum stress induced in TPU components are obtained.

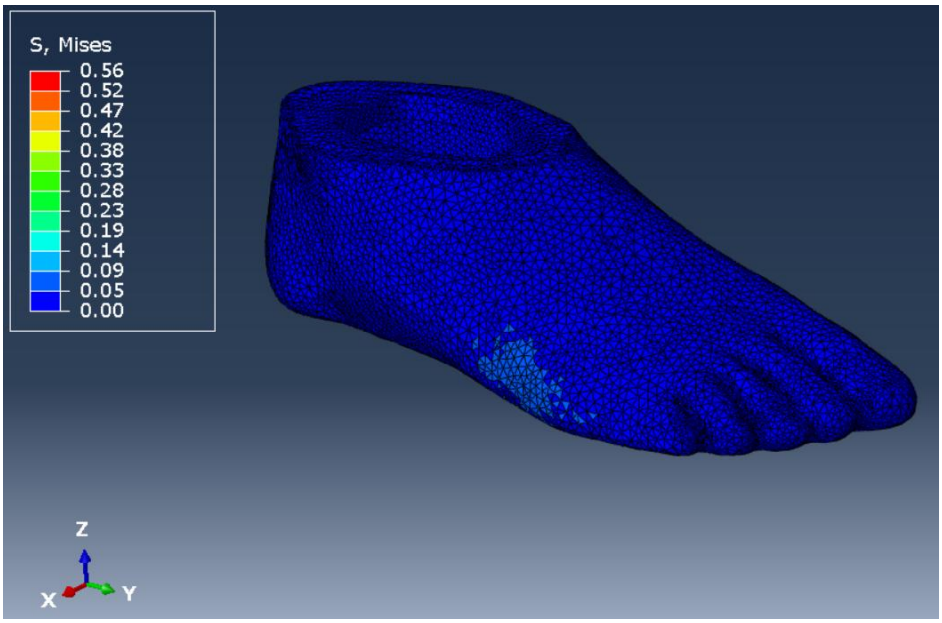

Figure 60: Von Mises stress of TPU components (inner foot and external cover).

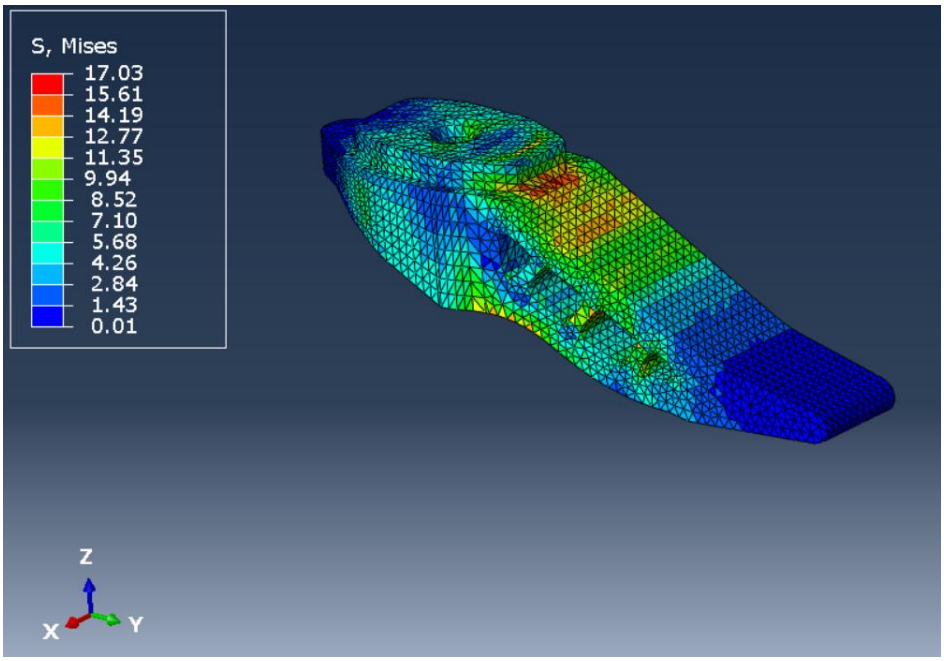

Figure 61: Von Mises stress of ABS Keel.

The Von-mises stress induced in the keel in mid-stance loading case is shown in Figure 61, with a maximum stress of 17MPa. The stress induced in keel in this case

is lower compared to the toe-off case, this is since the keel experiences a smaller bending moment during the loading case. If the keel is considered as a cantilever beam, point of application of load i.e., RP point is like the free end of the cantilever beam. In the case of toe-off case, the tip of the keel makes the contact first hence this acts as the fixed end whereas in case of mid-stance entire flat bottom surface makes contact. Therefore, the effective length between the contact and the point of application is smaller in mid-stance compared to the toe-off case, hence keel in mid-stance experiences lower bending moment and eventually lower stress than toe-off case. The deformation of prosthetic foot in mid-stance condition under the applied load is shown in Figure 62.

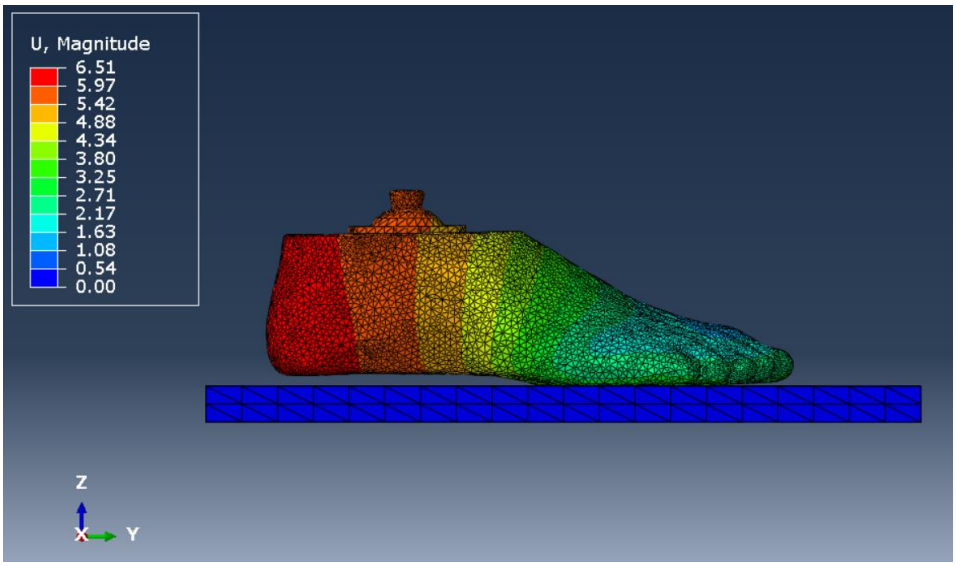

Figure 62: Deformation of prosthetic foot under applied load.

5.3 Heel-strike case

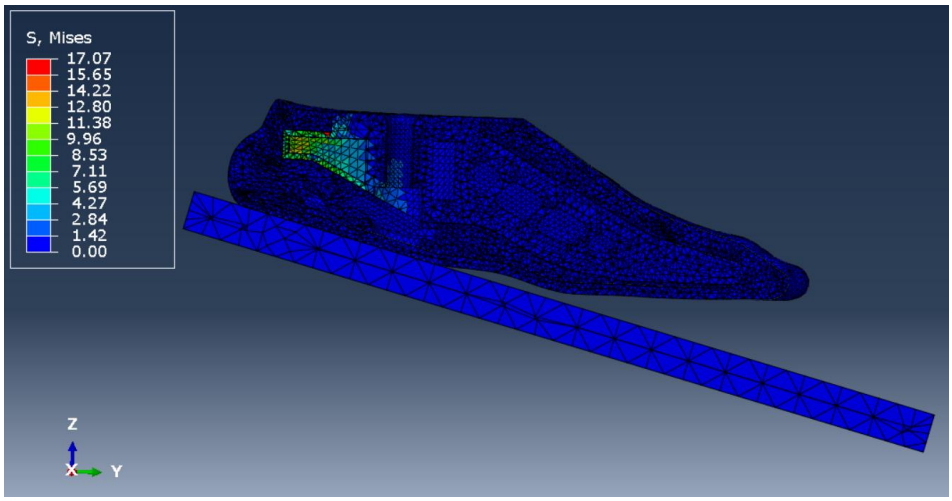

Figure 63: Von Mises stress of prosthetic foot (excluding pyramid connector and screw).

The von-mises stress induced on the rear side of the keel is higher than the other region as seen from the Figure 63 showing von-mises stress field in TPU components and keel together. The elements except those that belong to the rear part of the keel are in the blue color range which indicates the stresses are 1 to 2MPa. To obtain a clearer view about the von-mises stress induced in the TPU components alone, the keel elements are removed from the result view and are shown in Figure 64.

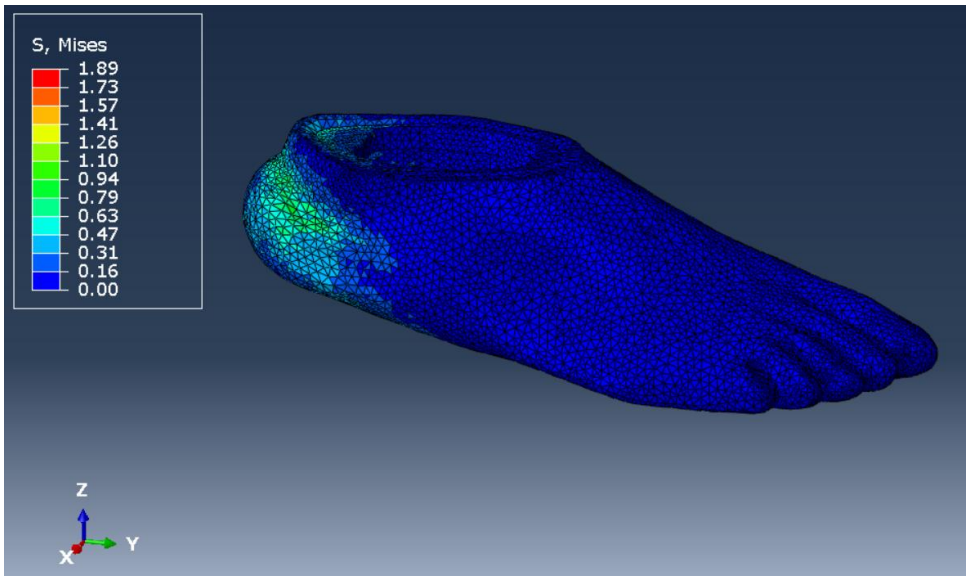

Figure 64: Von Mises stress of TPU components (inner foot and external cover).

The Von-mises stress plot shown in Figure 65 shows that the rear part of the keel is more stressful than the front part. The stresses in front part of the keel are in the range of 1 to 2MPa which is much lower compared to the 17.07MPa stress which

is induced in the rear side. Moreover, the deformation of the prosthetic foot under the applied load in the heel-strike condition is shown in Figure 66.

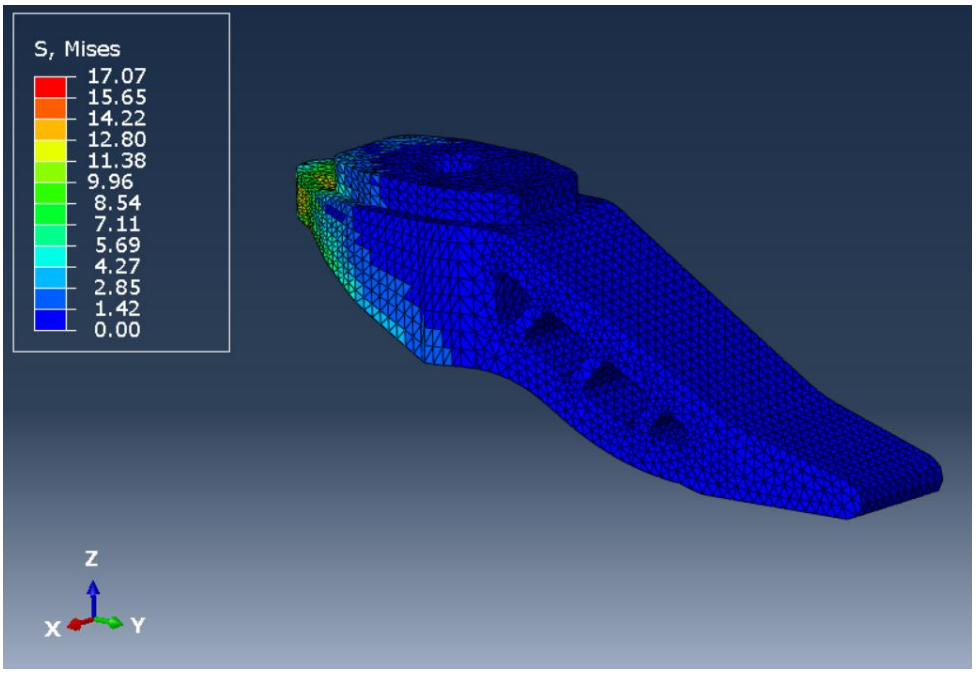

Figure 65: Von Mises stress of ABS Keel.

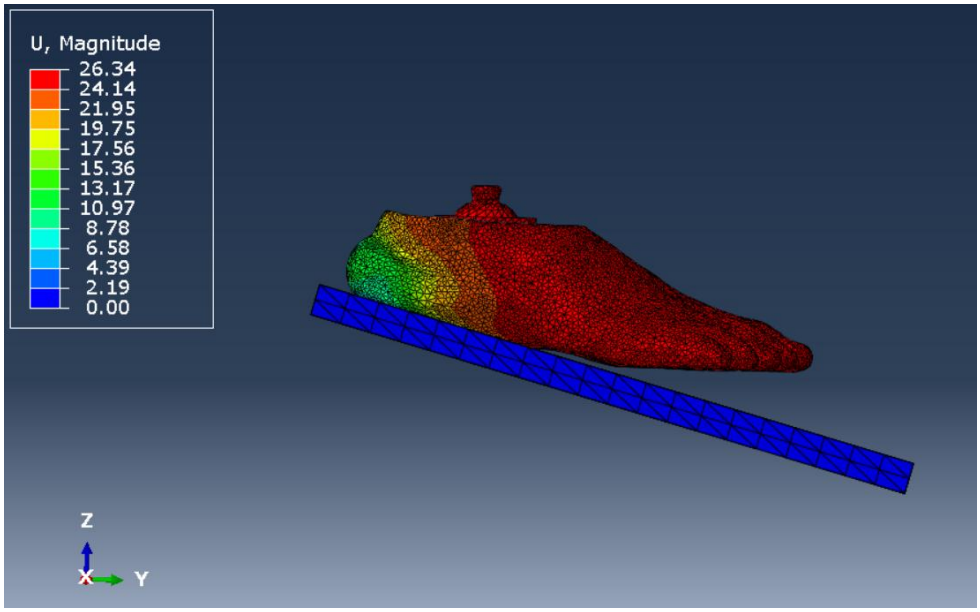

Figure 66: Deformation of prosthetic foot under applied load.

The maximum displacement measured at the reference point where the load of 2240N is applied in all three loading conditions are given in Table 5.

Table 5: Results from FEA at three loading cases.

Loading condition	Max deflection (at reference point)	Maximum stress induced in ABS component (Keel)	Maximum stress induced in TPU components (Inner foot and cover combined)
Toe-off	23.8 mm	25.6 MPa	2.08 MPa
Mid-stance	5.5 mm	17.03 MPa	0.56 MPa
Heel-strike	25.9 mm	17.07 MPa	1.89 MPa

The maximum deflection obtained from FEM analysis for the toe-off case is quite close to the experimental value (Table 1) provided by the Roadrunnerfoot Engineering company. In case of Heel-strike there is a difference in value obtained through FEM analysis and experimental value. And experimental value for the mid-stance case is not available with the company. The Roadrunnerfoot Engineering company was satisfied with the results listed in Table 5.

The maximum von-mises stress induced in the TPU components (inner foot and cover together) are in the range of 0.5 to 2MPa which is much lower than the ultimate tensile strength (UTS) of the material provided in table 4. Whereas in case of ABS keel, maximum von-mises stress induced are 25.6MPa, 17.03MPa and 17.07MPa for toe-off, mid-stance and heel-strike respectively. Considering all the loading cases, the maximum stress induced in the ABS component is 25.6 MPa, which is 1.4 MPa (approximately 5.2%) lower than the ultimate tensile strength (UTS) of the material with a safety factor of 1.05.

The ABS keel is used for the fatigue assessment of the prosthetic foot design as it experiences the highest stress compared to the inner foot and external cover. Additionally, ABS keel is most stressed in the toe-off condition. The principal stress obtained from the static assessment at the load of 1500N and 50N. The values corresponding to the load of 1500N and 50N are considered as maximum and minimum stress values. The mean (σ_m) and alternate (σ_a) stress components are estimated using the equations 5.1 and 5.2.

$$\sigma_m = \frac{\sigma_{max} + \sigma_{min}}{2} \tag{5.1}$$

$$\sigma_a = \frac{\sigma_{max} - \sigma_{min}}{2} \tag{5.2}$$

Table 6: Principal stresses estimated from Static FEA

Principal stress (MPa)	Maximum (MPa) At 1500N	Minimum (MPa) At 50N	Mean (MPa) σ_{im}	Alternate (MPa) σ_{ia}
σ1	6.59	0.20	3.40	3.19
σ2	19.86	0.65	10.25	9.61
σ3	4.52	0.2065	2.36	2.16

The principle, its corresponding Mean and Alternate stress components of the most stressed point in ABS keel is shown in Table 6. Fatigue behavior is assessed using Sines' criterion, as formulated in Equation 5.3.

$$\sigma_{Sa}^{*} = \sqrt{\sigma_{1a}^{2} + \sigma_{2a}^{2} + \sigma_{3a}^{2} - (\sigma_{1a} \cdot \sigma_{2a}) - (\sigma_{2a} \cdot \sigma_{3a}) - (\sigma_{1a} \cdot \sigma_{3a})} \leq \frac{1}{SF}\left[\sigma_{er} - \left(\frac{\sigma_{er}}{\sigma_{ep}} - 1\right) I_{m}\right] \quad (5.3)$$

Where,

- $\sigma_{1a}, \sigma_{2a}, and\ \sigma_{3a}$ are the alternate components of principle stress $\sigma_1, \sigma_2, and\ \sigma_3$ respectively.
- SF – safety factor
- σ_{er} - endurance limit from the fully reversed test (R = -1)
- σ_{ep} - endurance limit for pulsating loading (R = 0)
- I_m – sum of mean components of principle stresses

The endurance limit from the fully reversed test (σ_{er}) is determined using the Basquin formulation, as shown in Equations 5.4 and 5.5. The parameters log(A) and b, derived from experimental tests in a 2023 study [26], are 2.13 and -0.18, respectively. Assuming number of fatigue cycles (N) to be 2 million cycles (the minimum fatigue cycle required by ISO standards), the endurance limit (σ_{er}) from the fully reversed test is calculated as 9.9 MPa. Finally, using Equation 5.6, which defines the relationship between the endurance limit from the fully reversed test (σ_{er}) and the endurance limit for pulsating loading (σ_{ep}), σ_{ep} is estimated to be 7.25 MPa. Additionally, Equation 5.7 yields an I_m value of 16.01 MPa.

$$\sigma_{er} = A(N^b) \tag{5.4}$$

$$\log(\sigma_{er}) = \log(A) + b \cdot log(N) \tag{5.5}$$

$$\sigma_{ep} = \frac{\sigma_e}{(1 + \frac{\sigma_e}{UTS})} \tag{5.6}$$

$$I_m = \sigma_{1m} + \sigma_{2m} + \sigma_{3m} \tag{5.7}$$

It is possible to estimate the safety factor (SF) by knowing all the other parameters used in Equation 5.3, which is equal to 0.49. The Safety factor (SF) less than 1 indicates that the current design does not qualify the fatigue assessment under a cyclic load pulsating from 50N (min) to 1500N (max). Furthermore, by reducing the number of fatigue cycles (N) in the Basquin formulation from 2 million until the safety factor reaches 1, the fatigue life of the current design is estimated to be 42,956 cycles before failure. This is estimated with the help of excel solver function.

Finally, the results indicate that the prosthetic foot design withstands static loading in all three conditions—toe-off, mid-stance, and heel-strike—but fails under fatigue loading, with a lifespan of 42,956 cycles before failure. This suggests the need for a redesigning of the prosthetic foot or the consideration of alternate materials, which can be explored in future work

Chapter Six

6. Conclusions and Future work

In this study, a preliminary 3D-printed prosthetic foot design was analyzed to evaluate the feasibility of additive manufacturing in prosthetic applications. A combination of 2D and 3D analyses was conducted to assess the structural performance of a TPU-based prosthetic foot with and without an ABS keel.

The technical data sheet supplied by the manufacturer does not specify the Young's modulus of the TPU material. However, it provides three distinct stress-strain data points. By assuming a linear elastic behaviour for TPU, the Young's modulus is determined using a linear regression model based on these three stress-strain values.

The 2D analysis of the prosthetic foot made up of TPU showed high flexibility and resulted in a very high maximum deflection under the load. The young's modulus of ABS is approximately a thousand times the young's modulus of TPU. TPU prosthetic foot incorporated with ABS keel in the same 2D analysis showed significant increase in the stiffness of foot. The maximum deflection reduced by about 75% due to the addition of ABS keel in the prosthetic foot for the same applied load. The results of 2D analysis are quite accurate, which was ensured with the help of a simple convergence analysis.

The shape and size of the keel and inner foot are determined by the traditional iterative design approach. The keel was divided into two regions A and B, where three iterations are performed for region A, starting with a shorter length solid keel in the first iteration followed by a longer length solid keel and finally a hollow longer length keel with some volume reduction without violating maximum stress and deflection constraints. At the end of third iteration there was approximately 20% reduction in volume compared to the keel used in second iteration. A similar approach is used for the inner foot component.

Once the final design of all the components is completed, the components are assembled in Abaqus. The assembled prosthetic foot is subjected to three loading conditions namely toe-off, mid-stance and heel-strike, the boundary conditions and

load are in accordance with the ISO 10328: 2016 standard and P5 loading level. The 3D analysis confirmed that all components can endure the static load under all three loading conditions, with the stresses induced staying within the material's limits. The maximum deflection observed is within the acceptable range. The fatigue assessment of the current design fails to meet the number of fatigue cycles before failure prescribed by the ISO standard.

To conclude, this thesis showed how finite element analysis along with the optimization process while the design of the components showed that it is possible, from the theoretical point of view, to create a prosthetic device via additive manufacturing with the same stiffness as the conventionally manufactured one. The manufacturing time for the 3D-printed prosthetic foot is significantly shorter compared to the conventional method.

6.1 Future works:

- In this study, the TPU material was assumed to exhibit linear elastic behaviour. However, since TPU can also demonstrate hyper elastic characteristics, it would be more accurate to conduct simulations based on hyper elastic behaviour. Abaqus offers multiple models to represent hyper elasticity, making it essential to select the most suitable one for accurate results.
- In this study, the 3D prosthetic foot, assuming linear elastic material behaviour, was analyzed using the finite element method. To verify the accuracy of the FEM results, it is essential to build a prototype and conduct experimental testing under the same boundary and loading conditions.
- The fatigue assessment revealed that the current design does not meet the required number of fatigue cycles before failure as prescribed by the ISO standard. This necessitates redesigning the prosthetic foot or consideration of alternate materials. In any case it can lead to an increase in stiffness of the prosthetic foot which would require static proof test to ensure that the deflections are within the current acceptable range.
- The prosthetic foot is tested at specific three angles with respect to the horizontal axis, it would be better to test the design for the entire gait cycle.

Bibliography

[1] "what to know about prosthetic devices." URL: https://www.ottobock.com/en-ex/what-to-know-about-prosthetic-devices (visited on 2025).

[2] "Prosthetics through the ages." URL: shttps://magazine.medlineplus.gov/article/prosthetics-through-the-ages (visited on 2025).

[3] "Anatomy of the Foot" URL: https://www.arthritis.org/health-wellness/about-arthritis/where-it-hurts/anatomy-of-the-foot (visited on 2025).

[4] "Parts of a Prosthetic Leg" URL: https://www.ossur.com/en-us/prosthetics/information/parts-of-a-prosthetic-leg (visited on 2025).

[5] "Prosthetic feet." URL: https://www.physio-pedia.com/Prosthetic_Feet (visited on 2025).

[6] Pirker, W., Katzenschlager, R. Gait disorders in adults and the elderly. *Wien Klin Wochenschr* **129**, 81–95 (2017). https://doi.org/10.1007/s00508-016-1096-4.

[7] "Additive manufacturing process" URL: https://blog.spatial.com/additive-manufacturing-process (visited on 2025).

[8] "An Introduction to Additive Manufacturing (Also known as 3D printing) by Dr. Jason B. Jones." URL: https://additivemanufacturing.com/basics/ (visited on 2025).

[9] "A Guide to Additive Manufacturing" Damir Godec, Joamin Gonzalez-Gutierrez, Axel Nordin, Eujin Pei and Julia Ureña Alcázar. Springer Cham (2022) https://doi.org/10.1007/978-3-031-05863-9

[10] Kathrotiya, D., Yusuf, A., Bhagchandani, R.K. *et al.* A Study for the development of prosthetic foot by additive manufacturing. *J Braz. Soc. Mech. Sci. Eng.* **45**, 187 (2023). https://doi.org/10.1007/s40430-023-04107-y

[11] "3D Printable Thermoplastic Polyurethane Energy Efficient Passive Foot." Muhammad Hassaan Ahmed, Asharib Jamshid, Usman Amjad, Aashir Azhar, Muhammad, et al. 3D Printing and Additive Manufacturing 2022 9:6, 557-565. https://doi.org/10.1089/3dp.2021.0022

[12] "Design and Manufacture of a Customized Prosthetic Foot." Ines Jorge Ferreira. Instituto Superior T´ecnico, Lisboa, Portugal. May 2019.

[13] Ahmed MH, Jamshid A, Amjad U, et al. "3D Printable Thermoplastic Polyurethane Energy Efficient Passive Foot". 3D Print Addit Manuf. 2022 Dec 1;9(6):557-565. doi: 10.1089/3dp.2021.0022. Epub 2022 Dec 13. PMID: 36660747; PMCID: PMC9831569.

[14] "Effects of raster orientation, infill rate and infill pattern on the mechanical properties of 3D printed materials." Dudescu C, Racz L. Acta Univ Cibiniensis Tech Ser 2017;69: 23–30. DOI:10.1515/aucts-2017-0004

[15] "The effect of 3D printing temperature on the mechanical properties of polypropylene." Vo B, Ajibade A, Rosengren M, et al. Rapid Prototype J 2018;24, DOI: 10.1108/RPJ-04-2017-0055.
[16] Qi, H. J. and Boyce, M. C. [2005], 'Stress–strain behaviour of thermoplastic polyurethanes', Mechanics of Materials. **37**(8), 817–839.
[17] Tsukinovsky, D., Zaretsky, E. and Rutkevich, I. [1997], 'Material behaviour in plane polyurethane-polyurethane impact with velocities from 10 to 400 m/sec', Le Journal de Physique IV **7**(C3), C3–335.
[18] Elleuch, R., Elleuch, K., Salah, B. and Zahouani, H. [2007], 'Tribological behaviour of thermoplastic polyurethane elastomers', Materials & design **28**(3), 824–830.
[19] "Prosthetics - Structural testing of lower-limb prostheses. Requirements and test methods (ISO 10328: 2016)"
[20] "Concepts and Applications of Finite Element Analysis." Robert D. Cook, David S. Malkus. Third edition.
[21] "Adjusting surface to surface contact." URL: https://caeassistant.com/blog/adjusting-surface-to-surface-contact-abaqus-video/#:~:text=Master%20slave%20contact,surface)%20should%20be%20the%20master. (visited on 2025)
[22] https://recreus.com/gb/filaments/6-31-filaflex-70a.html#/1-colour-black/2-diameter-175_mm/3-weight-500_gr
[23] https://3d.nice-cdn.com/upload/file/TDS_hyper_ABS_EN_.pdf
[24] "Stiffness-driven design and optimization of a 3D-printed composite prosthetic foot: A beam finite Element-Based framework". March 2024. Abdel Rahman N. Al Thahabi, Luca M. Martulli, Andrea Bernasconi, et al. Composite Structures, Volume 337, 2024. https://doi.org/10.1016/j.compstruct.2024.118053
[25] "Numerical design and experimental validation of a 3D-printed composite energy-storage-and-return prosthetic foot". January 2025. Abdel Rahman N. Al Thahabi, Luca M. Martulli, Andrea Bernasconi, et al. Composite Structures, Volume 358, 2025. https://doi.org/10.1016/j.compstruct.2025.118907
[26] Yankin, A.; Serik, G.; et al. Optimization of Fatigue Performance of FDM ABS and Nylon Printed Parts. *Micromachines* **2023**, *14*, 304. https://doi.org/10.3390/mi14020304

List of Figures

Figure 1: Capua leg (replica). 4
Figure 2: An Artificial leg from American civil war 5
Figure 3: Anatomy of human foot. 5
Figure 4: Liner on the inner surface of socket. 7
Figure 5: Hydraulic knee joint, produced by Roadrunnerfoot Engineering. 7
Figure 6: An example of prosthetic SACH foot, produced by Ottobock 8
Figure 7: An example of prosthetic articulated feet, produced by Ottobock 8
Figure 8: An example of prosthetic articulated feet, produced by Ottobock 9
Figure 9: Phases of the normal gait cycle....10
Figure 10: Fused deposition modelling additive manufacturing types. 12
Figure 11: Prototype prostheses foot model....14
Figure 12: Nylon PA 12 foot. 15
Figure 13: 3D printed TPU foot. 15
Figure 14: 3D printed TPU foot with rigid PLA on the interior. 16
Figure 15: Stress vs strain of TPU 70 A. 18
Figure 16: ISO 10328: 2016 test procedure. 19
Figure 17: Toe-off condition in 2D analysis. 20
Figure 18: Mid-stance condition in 2D analysis. 20
Figure 19: Heel-strike condition in 2D analysis. 21
Figure 20: Plot showing Linear relation between quantity Φ and h^q. 22
Figure 21: Convergence chart. 23
Figure 22: 2D analysis on Toe-Off condition. 24
Figure 23: 2D analysis on Mid-Stance condition. 24
Figure 24: 2D analysis on Heel-Strike condition. 25
Figure 25: Force vs Displacement plot of Toe-off condition. 25
Figure 26: Force vs Displacement plot of Mid-Stance condition. 26
Figure 27: Force vs Displacement plot of Heel-Strike condition. 26
Figure 28: 2D Model with ABS keel (green) within the TPU 70A material (red) in toe-off condition. 27

Figure 29: 2D Toe-off case without ABS keel. 28
Figure 30: 2D Toe-off case with ABS keel. 28
Figure 31: Shorter length keel used in first iteration with an overall length of 215mm. 30
Figure 32: Inner foot. 31
Figure 33: External cover. 31
Figure 34: Pyramid connector. 32
Figure 35: Prosthetic foot assembly in toe-off case. Floor inclined at angle 20°. 33
Figure 36: cross-section in toe-off loading condition showing cover (green), inner foot (red), shorter length solid keel (pink), screw (blue), pyramid connector (grey) and floor contact (white) 33
Figure 37: Boundary and loading condition in toe-off case. 35
Figure 38: Boundary and loading condition in Mid-stance case. 35
Figure 39: Boundary and loading condition in heel-strike case. 36
Figure 40: Maximum deflection in toe-off case with shorter keel used in first iteration. 37
Figure 41: Longer length keel used in second iteration with an overall length of 241mm. 37
Figure 42: Maximum deflection in toe-off case with longer length keel used in the second iteration. 38
Figure 43: Keel divided into two regions A and B. 38
Figure 44: Variation of stress along the depth in keel. 39
Figure 45: Keel with cuts in region A used in third iteration. 39
Figure 46: Maximum deflection obtained in third iteration. 40
Figure 47: Final shape of Keel. 41
Figure 48: Assembled prosthetic foot with solid inner foot in heel-strike condition (left) and maximum deflection obtained in first iteration for inner foot (right). 41
Figure 49: Inner foot with one through cut (left) and maximum deflection obtained in second iteration for inner foot (right). 41
Figure 50: Inner foot with three cuts (left) and maximum deflection obtained in third iteration for inner foot (right). 42
Figure 51: Inner foot. 42
Figure 52: External cover. 43

Figure 53: Keel. 43
Figure 54: Pyramid connector. 44
Figure 55: Von Mises stress of prosthetic foot (excluding screw and pyramid connector). 45
Figure 56: Von Mises stress of TPU components (inner foot and external cover)....46
Figure 57: Von Mises stress of ABS Keel. The yellow circle showing location of maximum stress induced. 46
Figure 58: Deformation of prosthetic foot under applied load. 47
Figure 59: Von Mises stress of prosthetic foot (excluding the pyramid connector and screw). 47
Figure 60: Von Mises stress of TPU components (inner foot and external cover)....48
Figure 61: Von Mises stress of ABS Keel. 48
Figure 62: Deformation of prosthetic foot under applied load. 49
Figure 63: Von Mises stress of prosthetic foot (excluding pyramid connector and screw). 50
Figure 64: Von Mises stress of TPU components (inner foot and external cover)....50
Figure 65: Von Mises stress of ABS Keel. 51
Figure 66: Deformation of prosthetic foot under applied load. 51

List of Tables

Table 1: Static assessment experimental data from Roadrunnerfoot Engineering.....16
Table 2: Material properties.....18
Table 3: Convergence analysis data 23
Table 4: Material properties.....29
Table 5: Results from FEA at three loading cases.....52
Table 6: Principal stresses estimated from Static FEA 53